

Figure S1. Counterpart to Figure 5, showing valley response to sinusoidal variation in water supply at three forcing periods, for the cases where all sediment and water are supplied at the valley inlet (dashed lines, previously shown by M^cNab et al., 2023) and where sediment and water are supplied along stream with a power law exponent $p_{x,Q_w} = p_{x,Q_s} = 1.6$. (a–c) Blue solid line shows normalised variation in water supply as a function of time; dashed grey line shows normalised sediment discharge at the valley outlet for the upstream-supply case; solid black line shows normalised sediment discharge at the valley outlet for the along-stream supply case; greyscale circles show times used in panel (g–i). (d–f) Elevation, z , as a function of time for selected positions along stream, in response to changing water supply. Dashed grey lines represent upstream-supply case; solid, coloured lines represent along-stream supply case. (g–i) Valley long profiles for the along-stream supply case in response to changing water supply. Grey scale lines show long profiles, where shade corresponds to times represented by circles on panel (a–c); bluescale lines show perturbations from the steady state profile, δz .

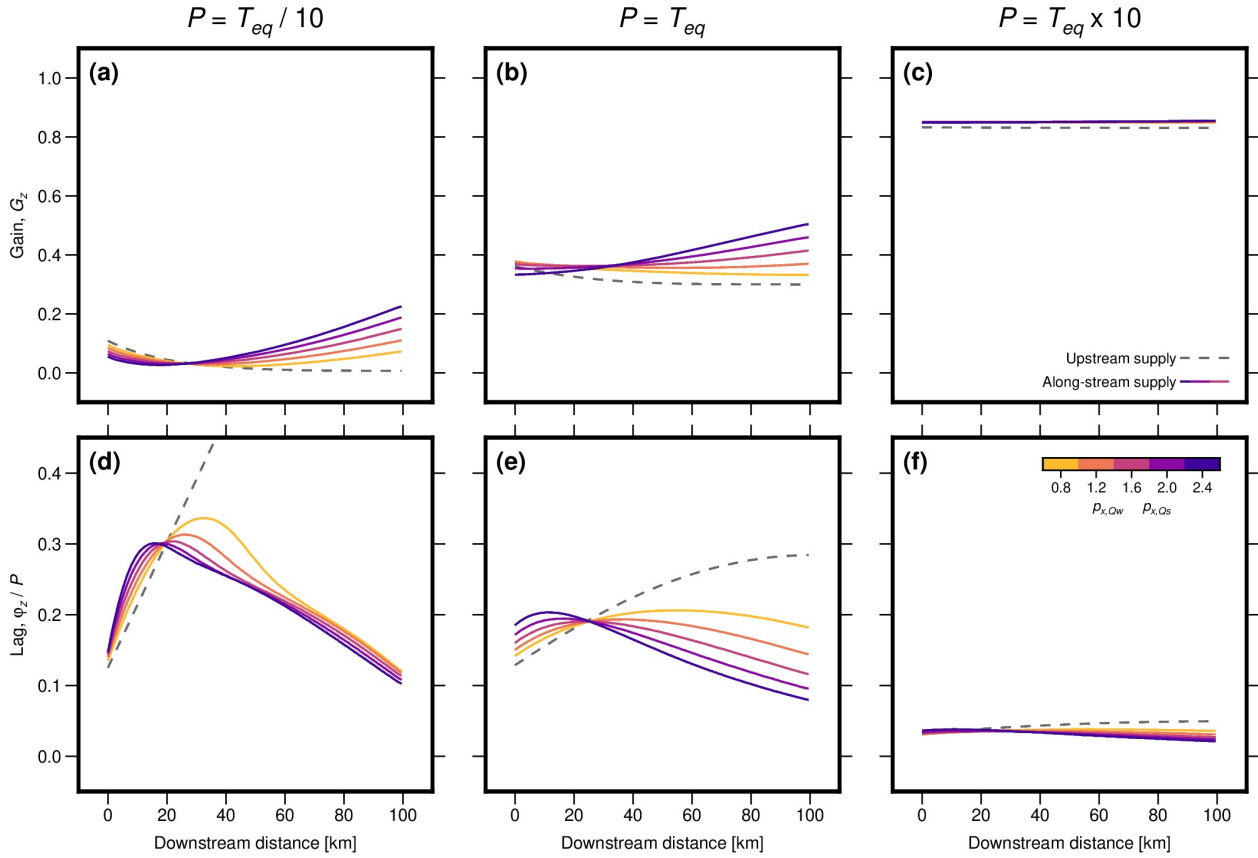


Figure S2. Counterpart to Figure 6, showing elevation gain, G_z , and lag, φ_z , of valley response to changing water supply, as functions of distance downstream for three forcing periods, $P = T_{eq}/10$ (a & d); $P = T_{eq}$ (b & e); $P = T_{eq} \times 10$ (c & f). Dashed grey lines show G_z and φ_z for the case where all sediment and water is supplied at the valley inlet (computed using the analytical expression given by M^cNab et al., 2023). Solid lines show G_z and φ_z for the case where sediment and water are supplied continuously along stream, where colour represents power-law exponent $p_{x,Qw} = p_{x,Qs}$. Note that the saturation of G_z at $6/7$ is related to the power of $7/6$ in the sediment-transport equation (Equation 2).

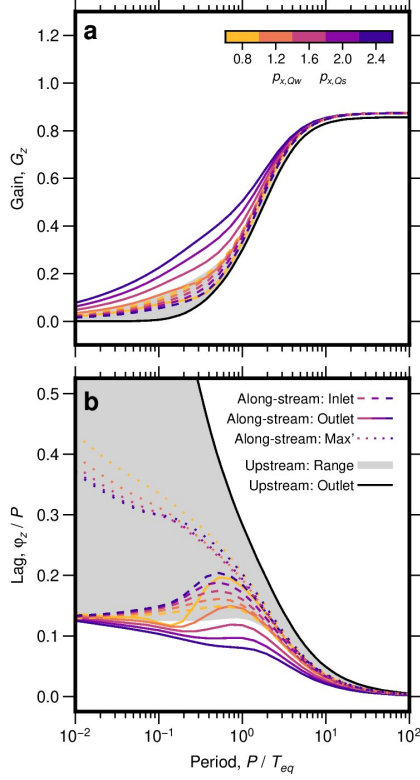


Figure S3. Counterpart to Figure 7, showing elevation gain and lag as a functions of forcing period for variation in water supply. (a) Elevation gain, G_z , as a function of forcing period, P . Black line and grey band show G_z at the valley outlet and its range throughout the valley, respectively, for the upstream supply case (computed using the analytical expression given by M^cNab et al., 2023). Solid and dashed coloured lines show G_z at the valley outlet and inlet, respectively, for the along-stream supply case, where colour represents power-law exponent $p_{x,Q_w} = p_{x,Q_s}$. (b) As (a) for elevation lag, ϕ_z . Additionally, dotted lines show maximum ϕ_z measured at any position along the valley for the along-stream supply case.

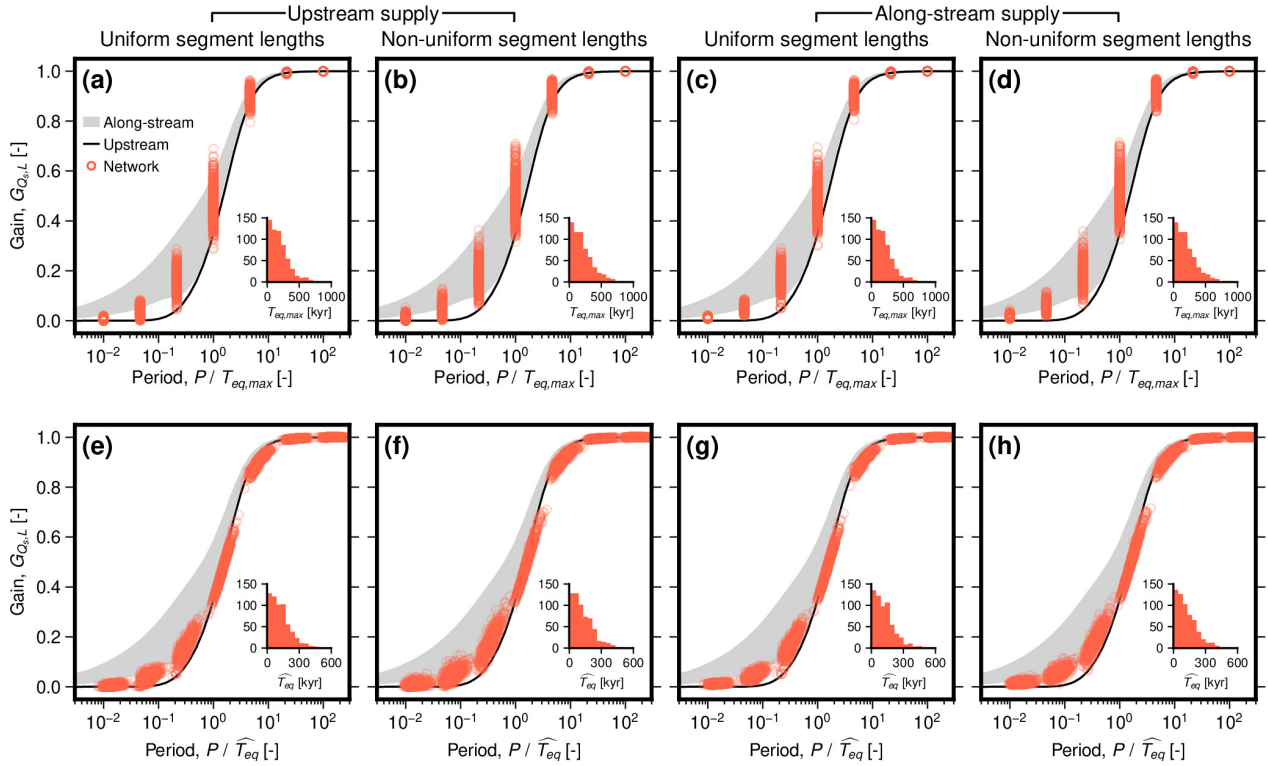


Figure S4. Counterpart to Figure 10, for the set of networks with number of inlet segments, $N_1 = 2-150$, showing gain for sediment discharge at the valley outlet, $G_{Q_s,L}$, as function of forcing period, P , normalised by equilibration time, T_{eq} . Circles represent networks, the black line represents the single segment case where all sediment and water are supplied at the inlet (M^cNab et al., 2023), and the grey band represents range for the single-segment case with along-stream supply of sediment and water, with power-law exponents p_{x,Q_w} and p_{x,Q_s} between 0.8 and 2.4. (a–d) T_{eq} defined using maximum length (i.e., maximum distance from valley inlet to outlet). (e–h) Empirical \widehat{T}_{eq} optimised for each network to minimise the difference between $G_{Q_s,L}$ as function of P/\widehat{T}_{eq} of the network and the upstream supply case. Inset histograms show distributions of obtained \widehat{T}_{eq} . (a,e) Uniform segment lengths with no along-stream supply of sediment and water; (b,f) non-uniform segment lengths with no along-stream supply of sediment and water; (c,g) uniform segment lengths with along-stream supply of sediment and water; (d,h) non-uniform segment lengths with along-stream supply of sediment and water.

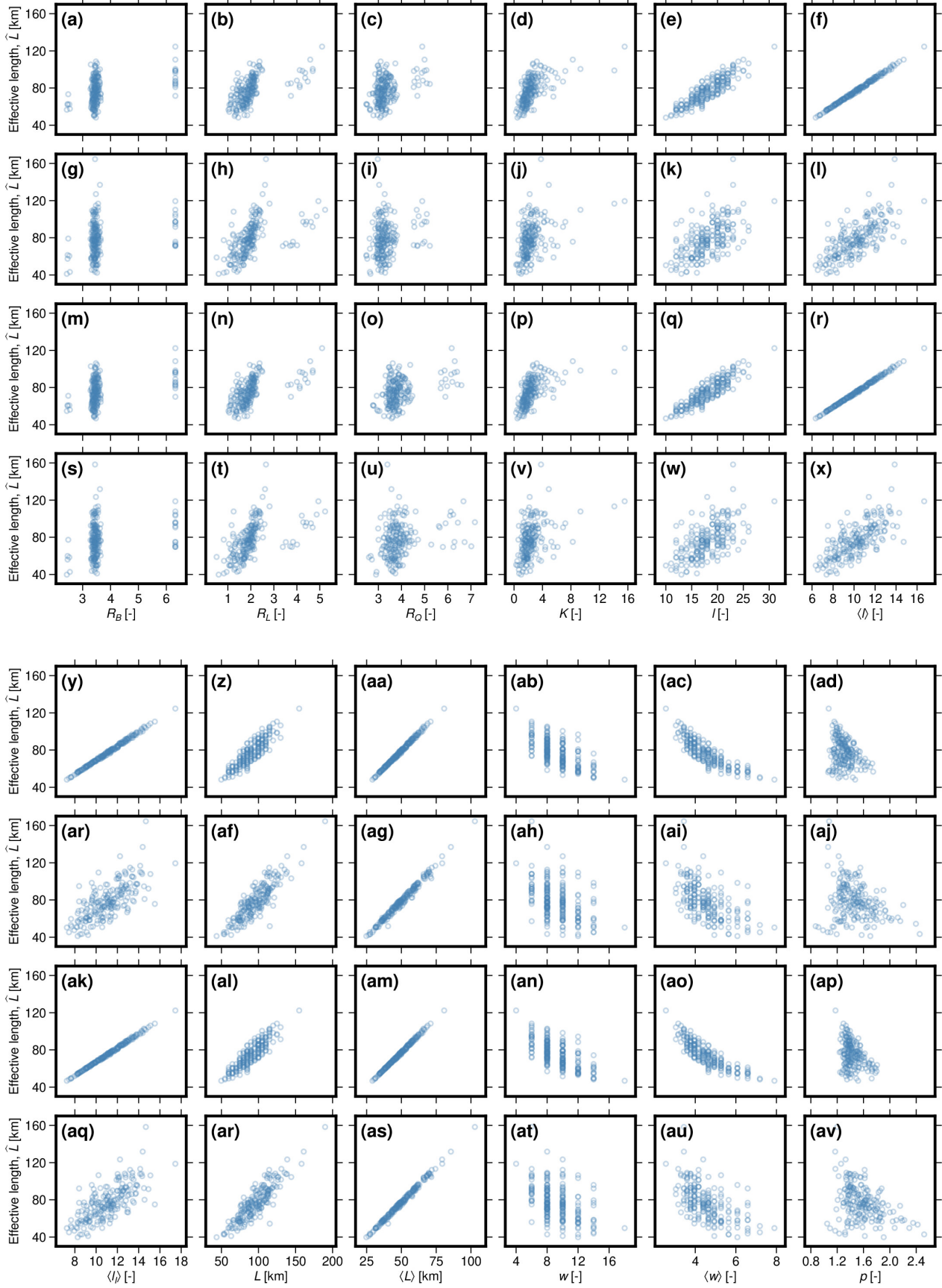


Figure S5. (Previous page.) Network effective length, \hat{L} , as function of various network properties for the set of networks with number of inlet segments, $N_1=40$. Four network scenarios are shown: (a–f) uniform segment lengths with no along-stream supply of sediment and water; (g–l) non-uniform segment lengths with no along-stream supply of sediment and water; (m–r) uniform segment lengths with along-stream supply of sediment and water; (s–x) non-uniform segment lengths with along-stream supply of sediment and water. (a, g, m, s) \hat{L} against bifurcation ratio, R_B . (b, h, n, t) \hat{L} against length ratio, R_L . (c, i, o, u) \hat{L} against discharge ratio, R_Q . (d, j, p, v) \hat{L} against Tokunaga's K . (e, k, q, w) \hat{L} against maximum topological length, l . (f, l, r, x) \hat{L} against mean topological length, $\langle l \rangle$. (y, ae, ak, aq) \hat{L} against mean inlet topological length, $\langle l_I \rangle$. (z, af, al, ar) \hat{L} against maximum length, L . (aa, ag, am, as) \hat{L} against mean length, $\langle L \rangle$. (ab, ah, an, at) \hat{L} against maximum topological width, w . (ac, ai, ao, au) \hat{L} against mean topological width, $\langle w \rangle$. (ad, aj, ap, av) \hat{L} against downstream distance–discharge exponent, p .

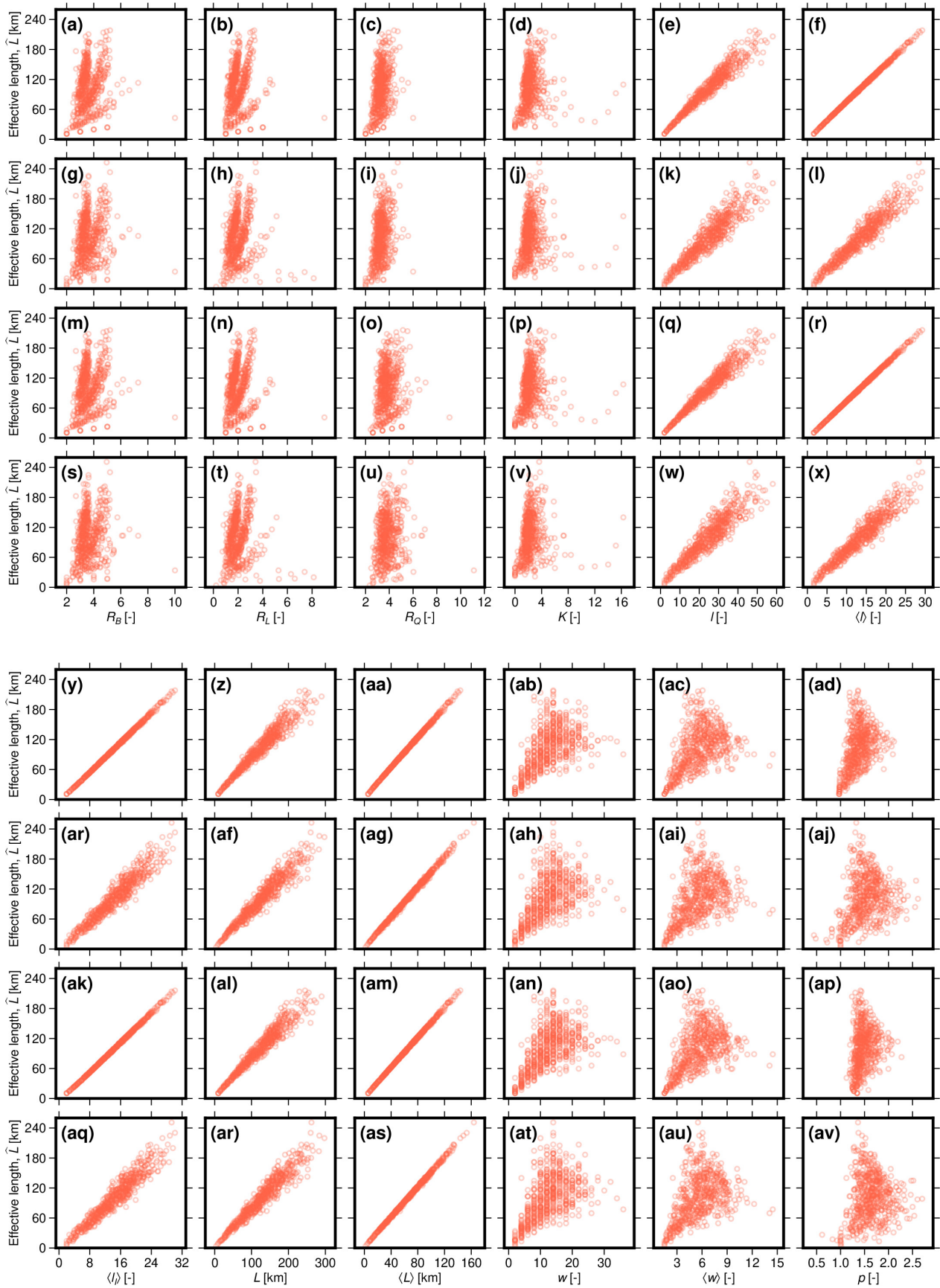


Figure S6. (Previous page.) Network effective length, \hat{L} , as function of various network properties for the set of networks with number of inlet segments, $N_1=2-150$. Four network scenarios are shown: (a–f) uniform segment lengths with no along-stream supply of sediment and water; (g–l) non-uniform segment lengths with no along-stream supply of sediment and water; (m–r) uniform segment lengths with along-stream supply of sediment and water; (s–x) non-uniform segment lengths with along-stream supply of sediment and water. (a, g, m, s) \hat{L} against bifurcation ratio, R_B . (b, h, n, t) \hat{L} against length ratio, R_L . (c, i, o, u) \hat{L} against discharge ratio, R_Q . (d, j, p, v) \hat{L} against Tokunaga's K . (e, k, q, w) \hat{L} against maximum topological length, l . (f, l, r, x) \hat{L} against mean topological length, $\langle l \rangle$. (y, ae, ak, aq) \hat{L} against mean inlet topological length, $\langle l_I \rangle$. (z, af, al, ar) \hat{L} against maximum length, L . (aa, ag, am, as) \hat{L} against mean length, $\langle L \rangle$. (ab, ah, an, at) \hat{L} against maximum topological width, w . (ac, ai, ao, au) \hat{L} against mean topological width, $\langle w \rangle$. (ad, aj, ap, av) \hat{L} against downstream distance–discharge exponent, p .

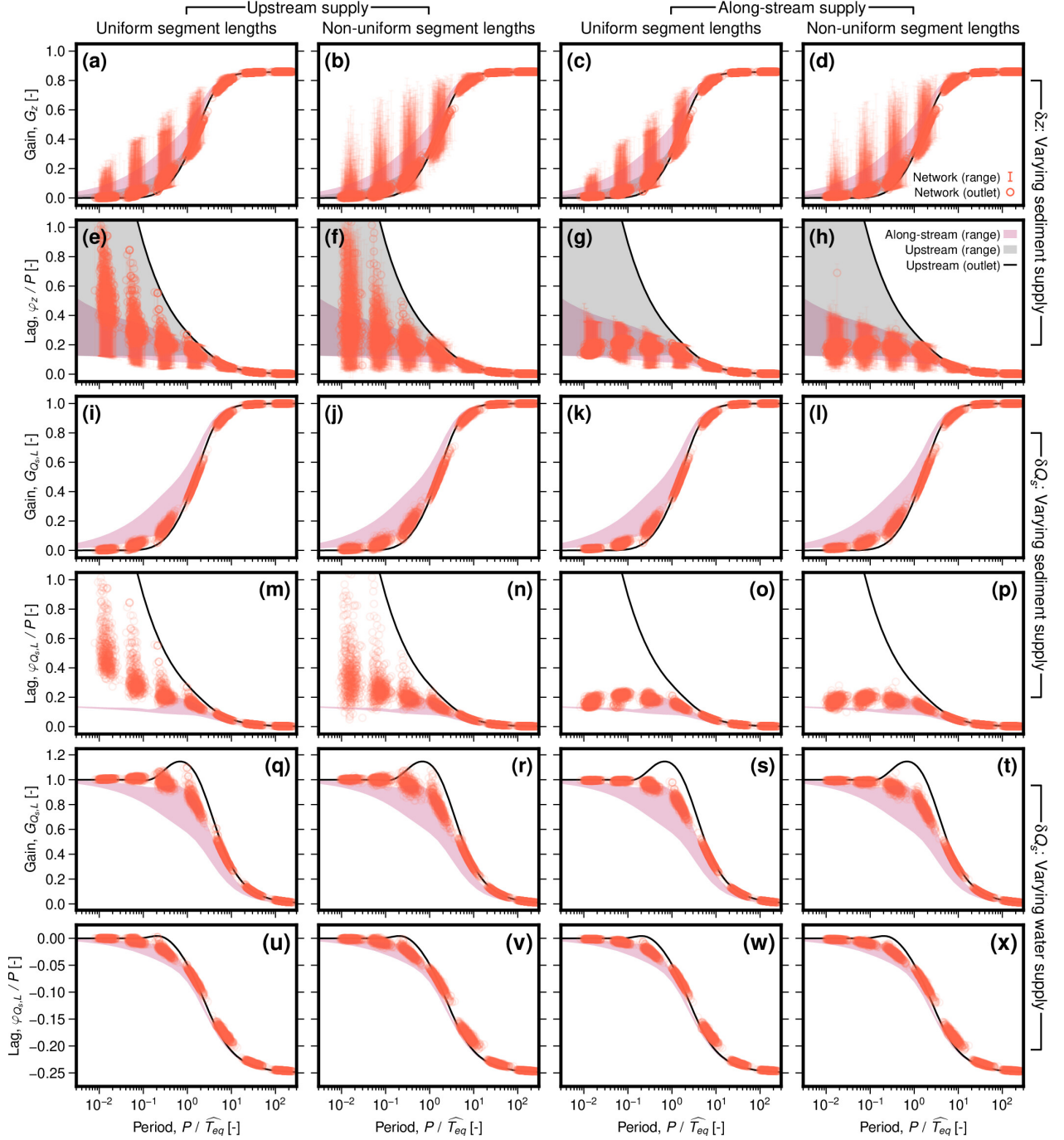


Figure S7. Counterpart to Figure 13, showing gain, G , and lag, φ , as functions of forcing period, P , normalised to empirical equilibration time, \widehat{T}_{eq} , for the set of networks with number of inlet segments, $N_1=2-150$. Four network scenarios are shown: (a,e,i,m,q,u) uniform segment lengths with no along-stream supply of sediment and water; (b,f,j,n,r,v) non-uniform segment lengths with no along-stream supply of sediment and water; (c,g,k,o,s,w) uniform segment lengths with along-stream supply of sediment and water; (d,h,l,p,t,x) non-uniform segment lengths with along-stream supply of sediment and water. (a–d) Elevation gain, G_z , in response to variation in sediment supply. Circles represent value at the network outlet, where error bars represent range throughout network. Black line and grey band represent value at outlet and range along stream, respectively, for simple case with all water and sediment supplied at the inlet (according to analytical solution of M^cNab et al., 2023). Pink band represents range along stream for simple case with along-stream supply of water and sediment, for power-law exponents $p_{x,Q_w} = p_{x,Q_s} = 0.8-2.4$. (e–h) As (a–d) for elevation lag. (i–p) As (a–h) for sediment-discharge gain, G_{Q_s} , and lag, φ_{Q_s} . Note that only values for the outlet are shown. Panels (i–l) are the same as Figure S4e–h. (q–x) As (i–p) for response to variation in water supply. Equivalent results to panels (a–h) for variation in water supply are shown in Figure S9.

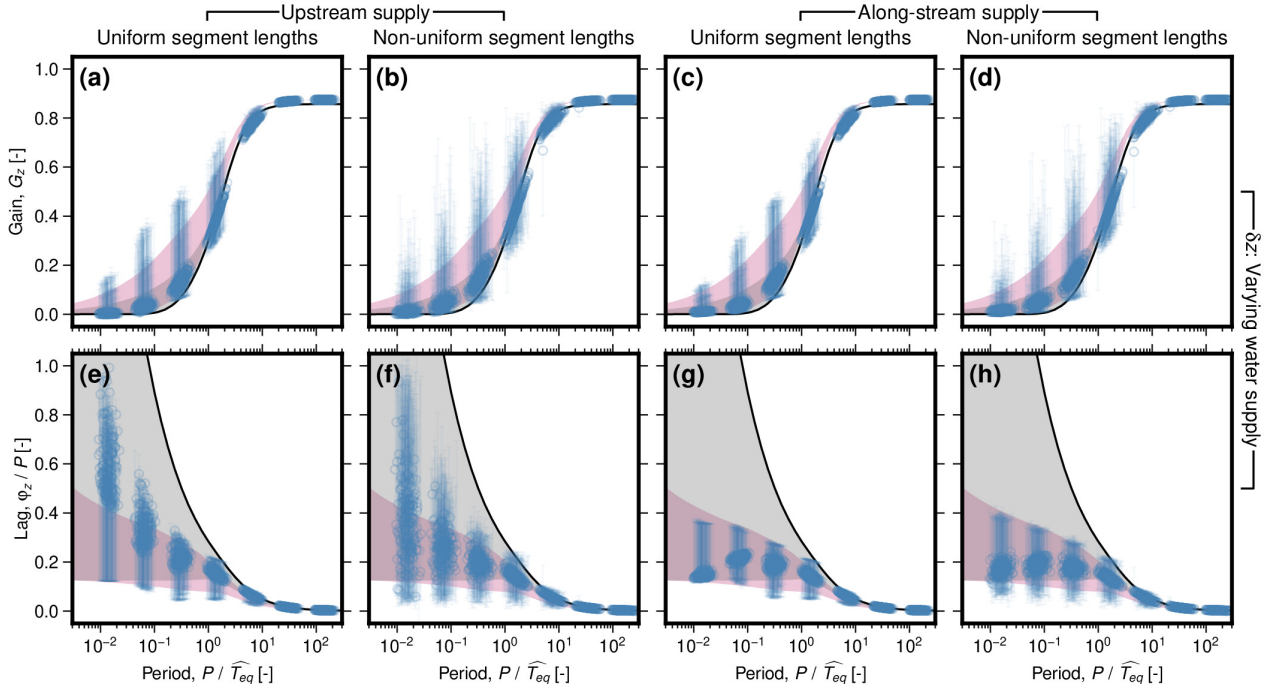


Figure S8. Counterpart to Figure 13, showing gain, G , and lag, φ , as functions of forcing period, P , normalised to empirical equilibration time, \widehat{T}_{eq} , for the set of networks with number of inlet segments, $N_1=40$. Four network scenarios are shown: (a,e) uniform segment lengths with no along-stream supply of sediment and water; (b,f) non-uniform segment lengths with no along-stream supply of sediment and water; (c,g) uniform segment lengths with along-stream supply of sediment and water; (d,h) non-uniform segment lengths with along-stream supply of sediment and water. (a–d) Elevation gain, G_z , in response to variation in water supply. Circles represent value at the network outlet, where error bars represent range throughout network. Black line and grey band represent value at outlet and range along stream, respectively, for simple case with all water and sediment supplied at the inlet (according to analytical solution of M^cNab et al., 2023). Pink band represents range along stream for simple case with along-stream supply of water and sediment, for power-law exponents $p_{x,Q_w} = p_{x,Q_s} = 0.8\text{--}2.4$. (e–h) As (a–d) for elevation lag.

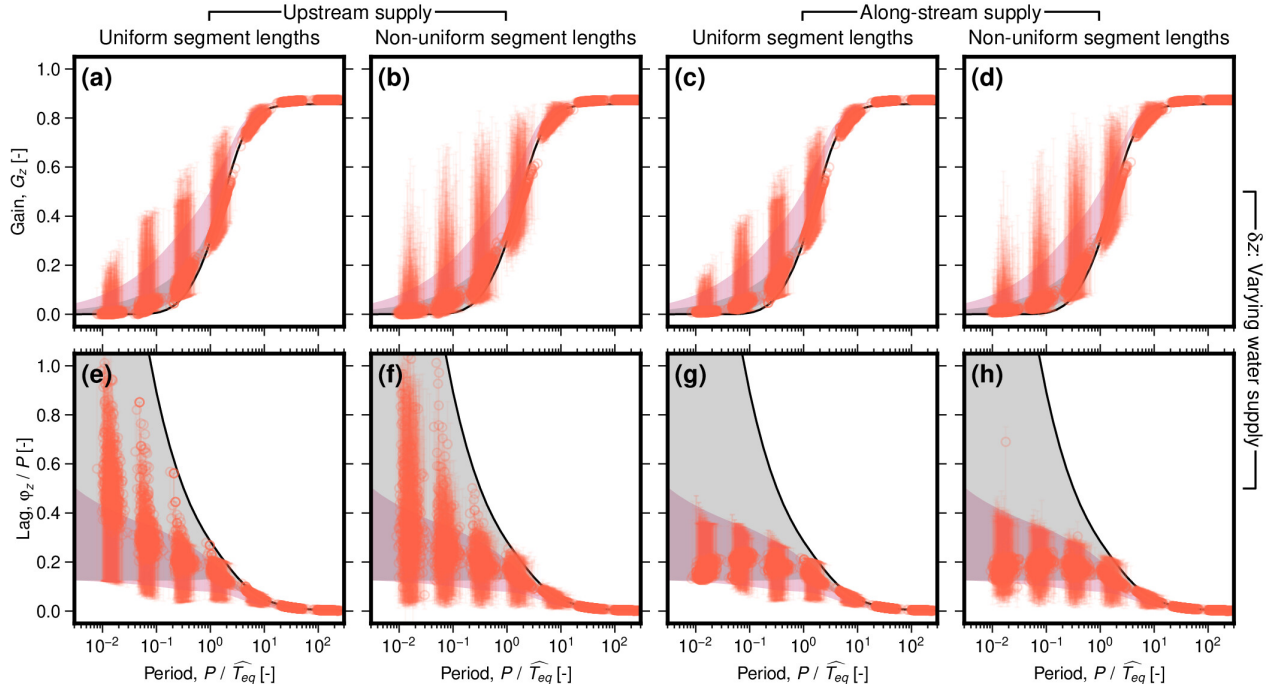


Figure S9. Counterpart to Figure 13, showing gain, G , and lag, φ , as functions of forcing period, P , normalised to empirical equilibration time, \hat{T}_{eq} , for the set of networks with number of inlet segments, $N_1=2-150$. Four network scenarios are shown: (a,e) uniform segment lengths with no along-stream supply of sediment and water; (b,f) non-uniform segment lengths with no along-stream supply of sediment and water; (c,g) uniform segment lengths with along-stream supply of sediment and water; (d,h) non-uniform segment lengths with along-stream supply of sediment and water. (a–d) Elevation gain, G_z , in response to variation in water supply. Circles represent value at the network outlet, where error bars represent range throughout network. Black line and grey band represent value at outlet and range along stream, respectively, for simple case with all water and sediment supplied at the inlet (according to analytical solution of M^cNab et al., 2023). Pink band represents range along stream for simple case with along-stream supply of water and sediment, for power-law exponents $p_{x,Q_w} = p_{x,Q_s} = 0.8-2.4$. (e–h) As (a–d) for elevation lag.

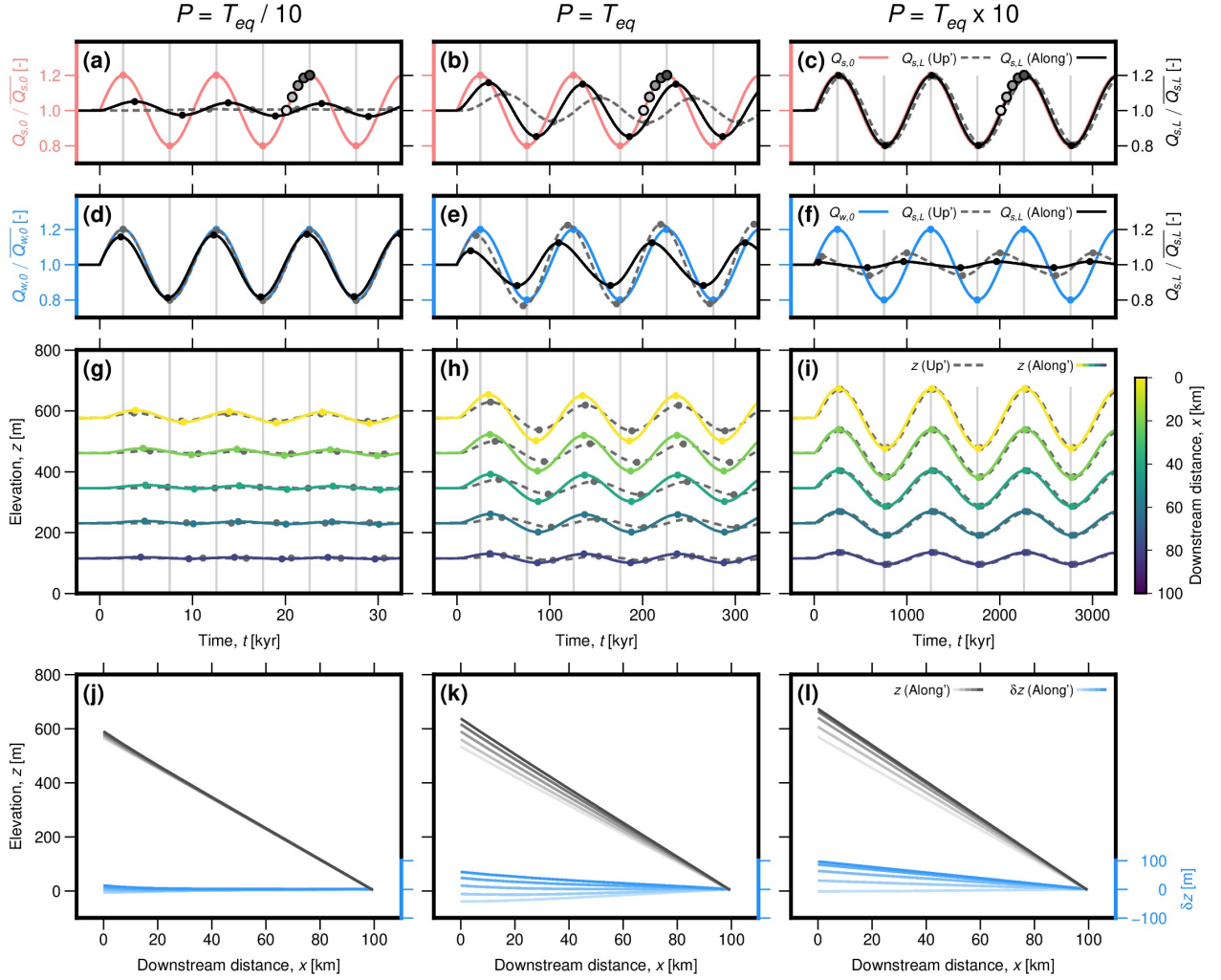


Figure S10. Counterpart to Figure 5, where valley width, B , increases downstream at the same rate as water discharge, Q_w , rather than being spatially uniform. Valley response to sinusoidal variation in sediment and water supply at three forcing periods is shown, for the cases where all sediment and water are supplied at the valley inlet (dashed lines, previously shown by M^cNab et al., 2023) and where sediment and water are supplied along stream with a power law exponent $p_{x,Q_w} = p_{x,Q_s} = 1.6$. (a–c) Red solid line shows normalised variation in sediment supply as a function of time; dashed grey line shows normalised sediment discharge at the valley outlet for the upstream-supply case; solid black line shows normalised sediment discharge at the valley outlet for the along-stream supply case; greyscale circles show times used in panel (j–l). (d–f) Same as (a–c) except blue solid line shows normalised variation in water supply. (g–i) Elevation, z , as a function of time for selected positions along stream, in response to changing sediment supply. Dashed grey lines represent upstream-supply case; solid, coloured lines represent along-stream supply case. (j–l) Valley long profiles at different times for the along-stream supply case in response to changing sediment supply (for the upstream supply case, compare with Figures 2 and 3 in M^cNab et al., 2023). Grey scale lines show long profiles, where shade corresponds to times represented by circles on panel (a–c); bluescale lines show perturbations from the steady state profile, δz . Equivalents to panels (g–l) for variation in water supply are shown in Figure S11.

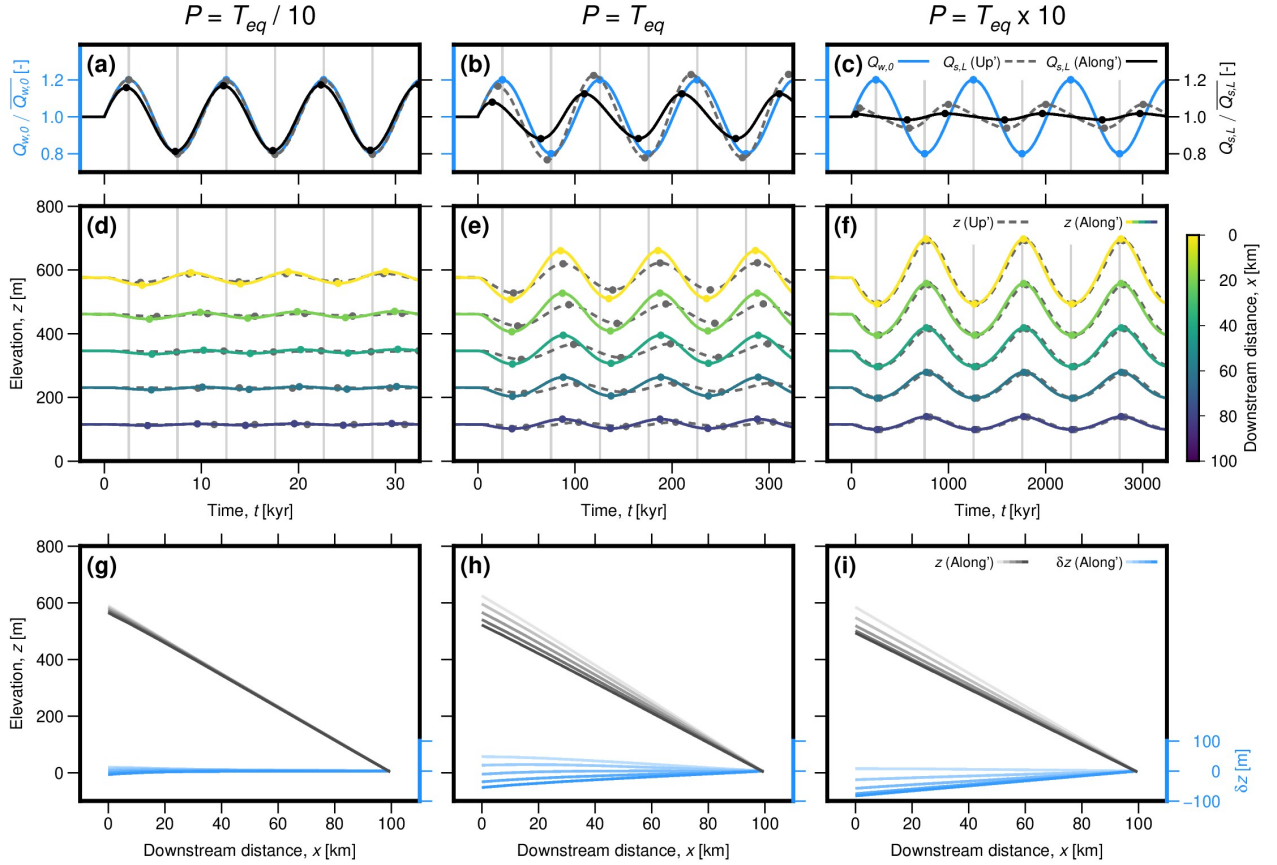


Figure S11. Counterpart to Figure S1, where valley width, B , increases downstream at the same rate as water discharge, Q_w , rather than being spatially uniform. Valley response to sinusoidal variation in water supply at three forcing periods is shown for the cases where all sediment and water are supplied at the valley inlet (dashed lines, previously shown by M^cNab et al., 2023) and where sediment and water are supplied along stream with a power law exponent $p_{x,Q_w} = p_{x,Q_s} = 1.6$. (a–c) Blue solid line shows normalised variation in water supply as a function of time; dashed grey line shows normalised sediment discharge at the valley outlet for the upstream-supply case; solid black line shows normalised sediment discharge at the valley outlet for the along-stream supply case; greyscale circles show times used in panel (g–i). (d–f) Elevation, z , as a function of time for selected positions along stream, in response to changing water supply. Dashed grey lines represent upstream-supply case; solid, coloured lines represent along-stream supply case. (g–i) Valley long profiles at different times for the along-stream supply case in response to changing water supply. Grey scale lines show long profiles, where shade corresponds to times represented by circles on panel (a–c); bluescale lines show perturbations from the steady state profile, δz .

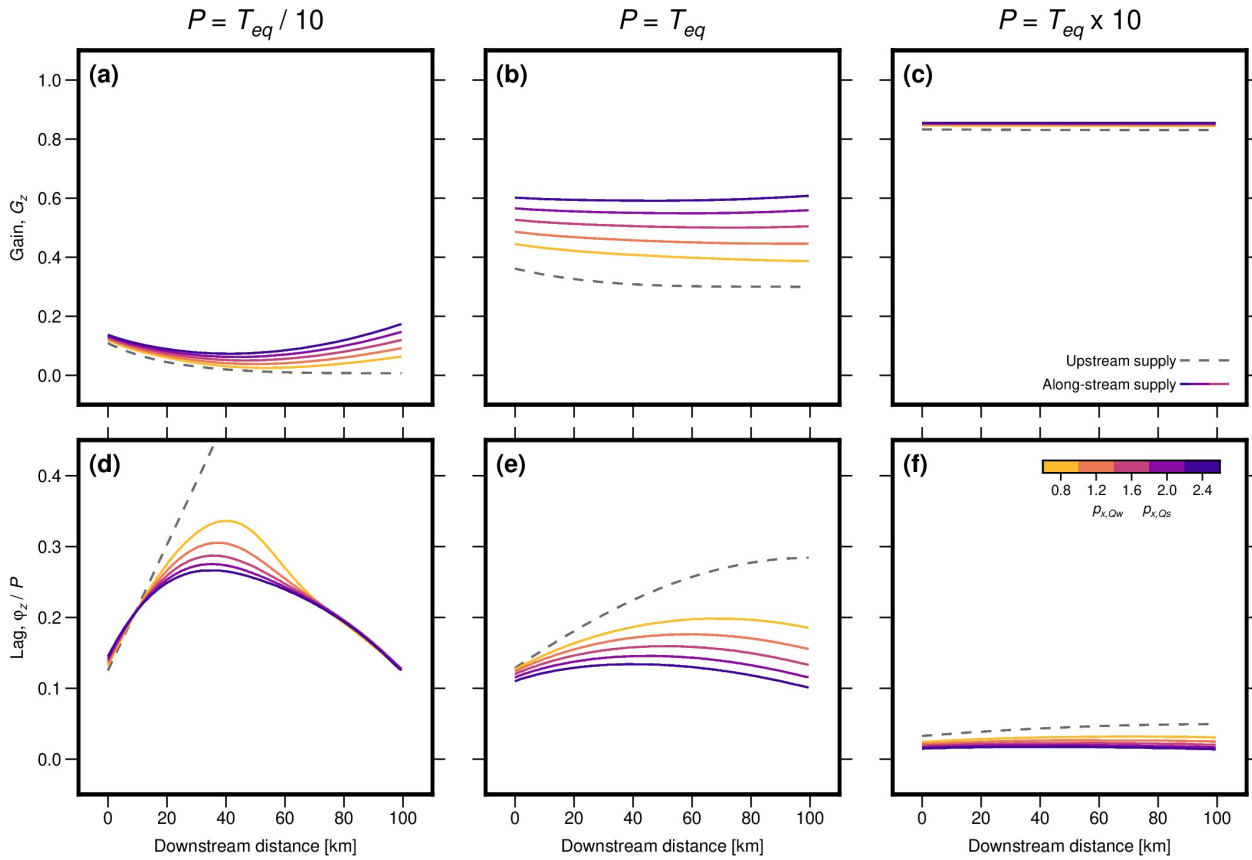


Figure S12. Counterpart to Figure 6, where valley width, B , increases downstream at the same rate as water discharge, Q_w , rather than being spatially uniform. Elevation gain, G_z , and lag, φ_z , of valley response to changing sediment supply are shown, as functions of distance downstream for three forcing periods, $P = T_{eq}/10$ (a & d); $P = T_{eq}$ (b & e); $P = T_{eq} \times 10$ (c & f). Dashed grey lines show G_z and φ_z for the case where all sediment and water is supplied at the valley inlet (computed using the analytical expression given by M^cNab et al., 2023). Solid lines show G_z and φ_z for the case where sediment and water are supplied continuously along stream, where colour represents power-law exponent $p_{x,Qw} = p_{x,Qs}$. Note that the saturation of G_z at $6/7$ is related to the power of $7/6$ in the sediment-transport equation (Equation 2). The behaviour in response to changing water supply is very similar (Figure S13).

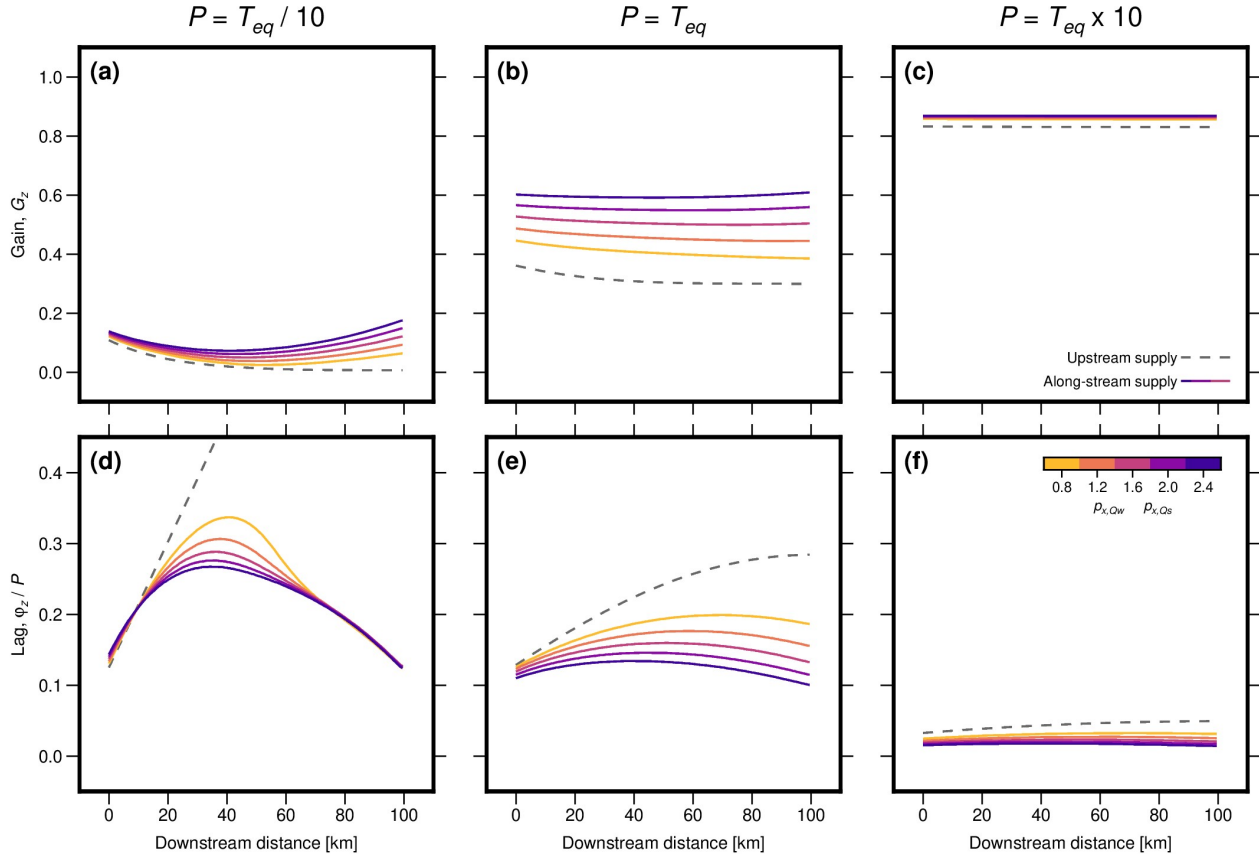


Figure S13. Counterpart to Figure S2, where valley width, B , increases downstream at the same rate as water discharge, Q_w , rather than being spatially uniform. Elevation gain, G_z , and lag, φ_z , of valley response to changing water supply are shown, as functions of distance downstream for three forcing periods, $P = T_{eq}/10$ (a & d); $P = T_{eq}$ (b & e); $P = T_{eq} \times 10$ (c & f). Dashed grey lines show G_z and φ_z for the case where all sediment and water is supplied at the valley inlet (computed using the analytical expression given by M^cNab et al., 2023). Solid lines show G_z and φ_z for the case where sediment and water are supplied continuously along stream, where colour represents power-law exponent $p_{x,Qw} = p_{x,Qs}$. Note that the saturation of G_z at $6/7$ is related to the power of $7/6$ in the sediment-transport equation (Equation 2).

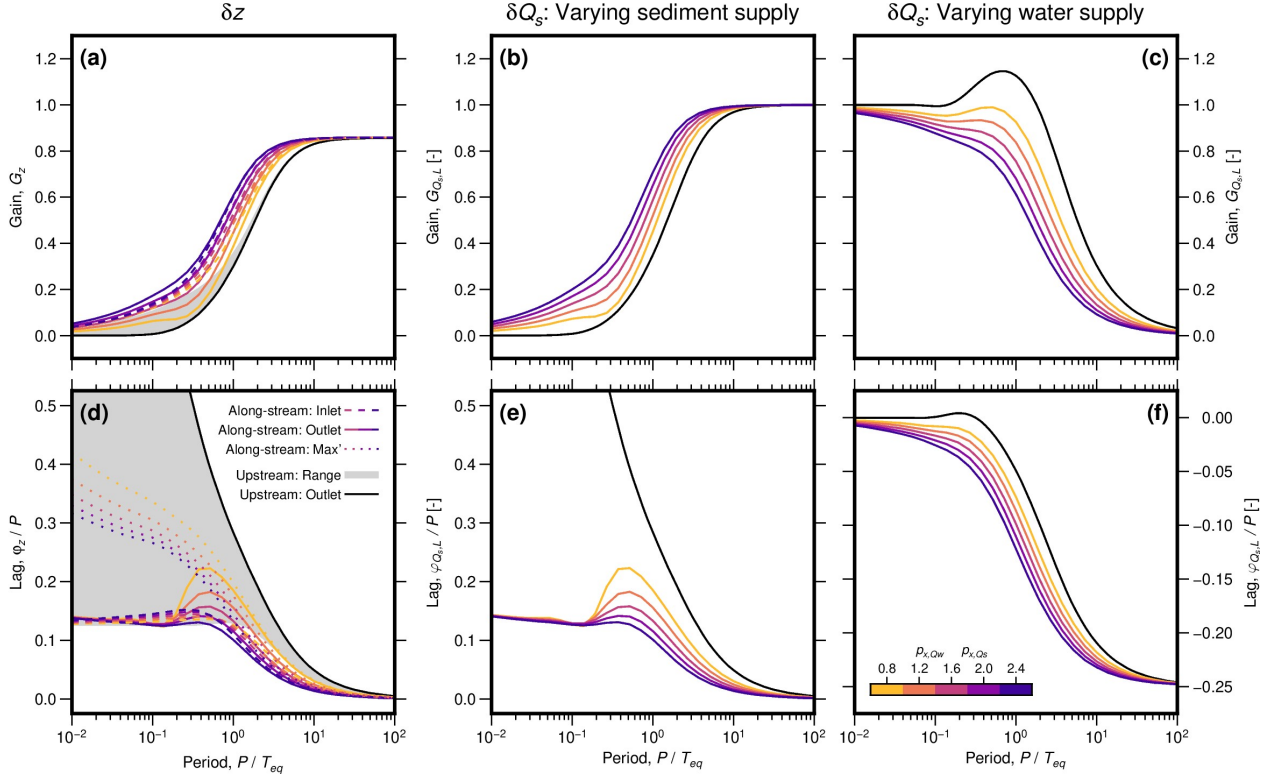


Figure S14. Counterpart to Figure 7, where valley width, B , increases downstream at the same rate as water discharge, Q_w , rather than being spatially uniform. Gain and lag are shown as functions of forcing period. (a) Elevation gain, G_z , as a function of forcing period, P . Black line and grey band show G_z at the valley outlet and its range throughout the valley, respectively, for the upstream supply case (computed using the analytical expression given by M^cNab et al., 2023). Solid and dashed coloured lines show G_z at the valley outlet and inlet, respectively, for the along-stream supply case, where colour represents power-law exponent $p_{x,Q_w} = p_{x,Q_s}$. (b & c) As (a) for variation in sediment discharge at the outlet, $G_{Q_s,L}$, in response to varying sediment and water supply, respectively. (d) As (a) for elevation lag, φ_z . Additionally, dotted lines show maximum φ_z measured at any position along the valley for the along-stream supply case. Equivalents to panels (a & d) for variation in water supply are shown in Figure S3. (e & f) As (d) for variation in sediment discharge at the outlet, $\varphi_{Q_s,L}$, in response to varying sediment and water supply, respectively.

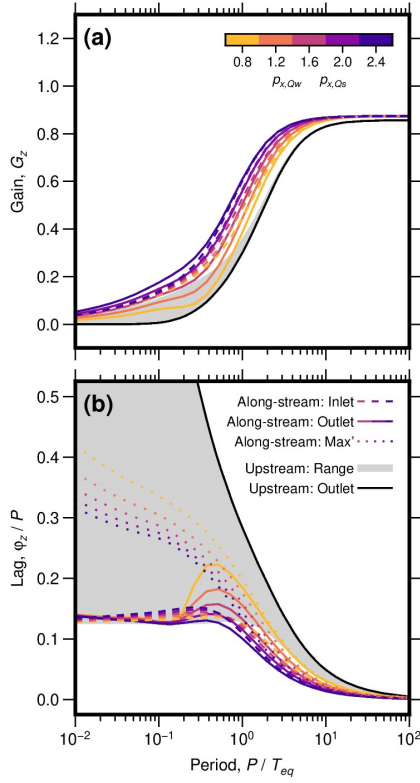


Figure S15. Counterpart to Figure S3, where valley width, B , increases downstream at the same rate as water discharge, Q_w , rather than being spatially uniform. Elevation gain and lag are shown as functions of forcing period for variation in water supply. (a) Elevation gain, G_z , as a function of forcing period, P . Black line and grey band show G_z at the valley outlet and its range throughout the valley, respectively, for the upstream supply case (computed using the analytical expression given by McNab et al., 2023). Solid and dashed coloured lines show G_z at the valley outlet and inlet, respectively, for the along-stream supply case, where colour represents power-law exponent $p_{x, Q_w} = p_{x, Q_s}$. (b) As (a) for elevation lag, φ_z . Additionally, dotted lines show maximum φ_z measured at any position along the valley for the along-stream supply case.

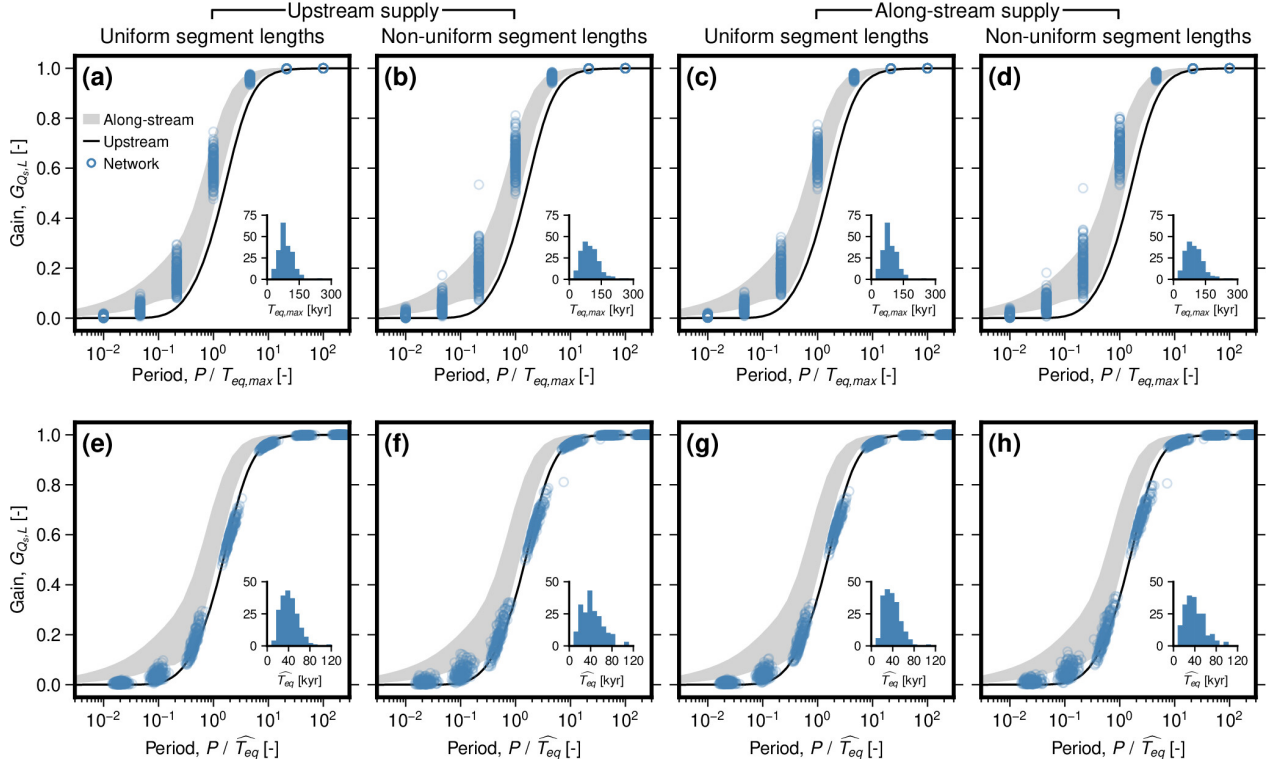


Figure S16. Counterpart to Figure 10, where valley width, B , increases downstream at the same rate as water discharge, Q_w , rather than being spatially uniform. Gain for sediment discharge at the valley outlet, $G_{Q_s,L}$, is shown as function of forcing period, P , normalised by equilibration time, T_{eq} , for the set of networks with number of inlet segments, $N_1=40$. Circles represent networks, the black line represents the single segment case where all sediment and water are supplied at the inlet (M^cNab et al., 2023), and the grey band represents range for the single-segment case with along-stream supply of sediment and water, with power-law exponents p_{x,Q_w} and p_{x,Q_s} between 0.8 and 2.4. (a–d) T_{eq} defined using maximum length (i.e., maximum distance from valley inlet to outlet). (e–h) Empirical \hat{T}_{eq} optimised for each network to minimise the difference between $G_{Q_s,L}$ as function of P/T_{eq} of the network and the upstream supply case. Inset histograms show distributions of obtained \hat{T}_{eq} . (a,e) Uniform segment lengths with no along-stream supply of sediment and water; (b,f) non-uniform segment lengths with no along-stream supply of sediment and water; (c,g) uniform segment lengths with along-stream supply of sediment and water; (d,h) non-uniform segment lengths with along-stream supply of sediment and water. Equivalent results for the set of networks with $N_1=2-150$ are shown in Figure S17.

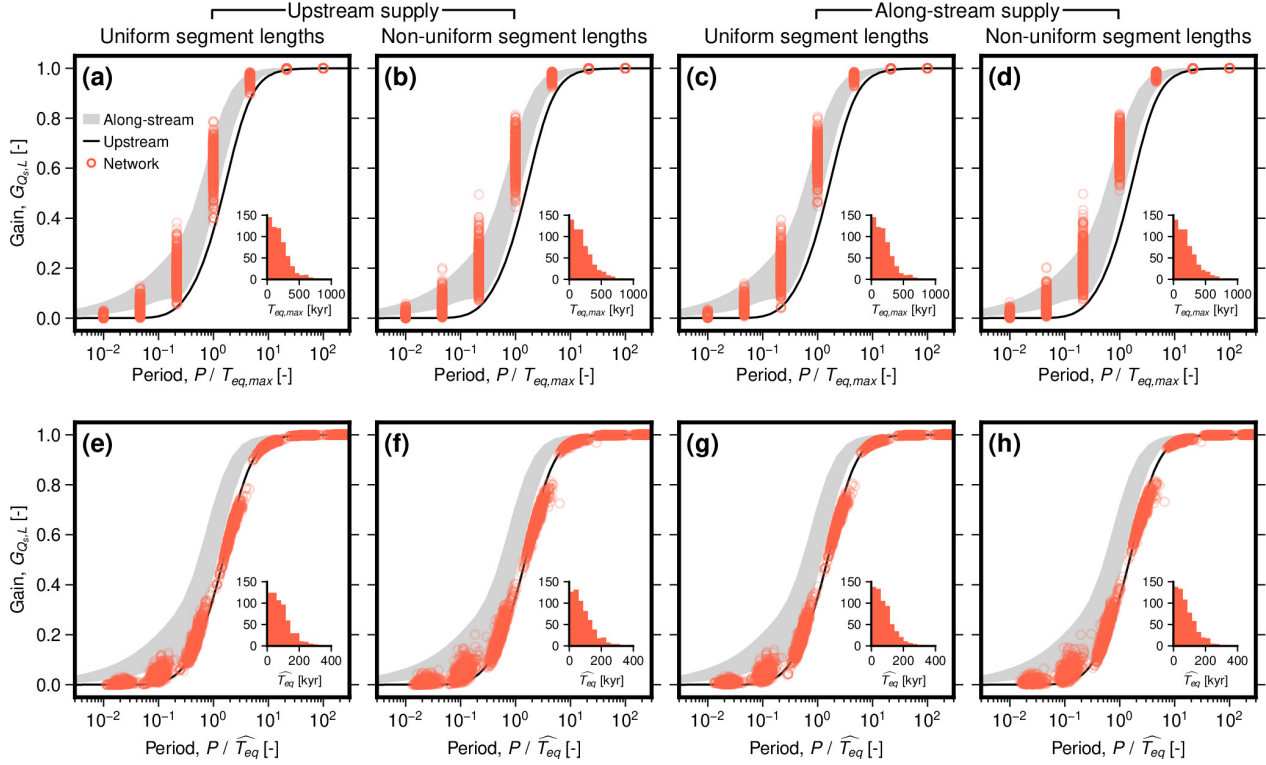


Figure S17. Counterpart to Figure S4, where valley width, B , increases downstream at the same rate as water discharge, Q_w , rather than being spatially uniform. Gain for sediment discharge at the valley outlet, $G_{Q_{s,L}}$, is shown as function of forcing period, P , normalised by equilibration time, T_{eq} , for the set of networks with number of inlet segments, $N_1=2-150$. Circles represent networks, the black line represents the single segment case where all sediment and water are supplied at the inlet (McNab et al., 2023), and the grey band represents range for the single-segment case with along-stream supply of sediment and water, with power-law exponents p_{x,Q_w} and p_{x,Q_s} between 0.8 and 2.4. (a–d) T_{eq} defined using maximum length (i.e., maximum distance from valley inlet to outlet). (e–h) Empirical \hat{T}_{eq} optimised for each network to minimise the difference between $G_{Q_{s,L}}$ as function of P/T_{eq} of the network and the upstream supply case. Inset histograms show distributions of obtained \hat{T}_{eq} . (a,e) Uniform segment lengths with no along-stream supply of sediment and water; (b,f) non-uniform segment lengths with no along-stream supply of sediment and water; (c,g) uniform segment lengths with along-stream supply of sediment and water; (d,h) non-uniform segment lengths with along-stream supply of sediment and water.

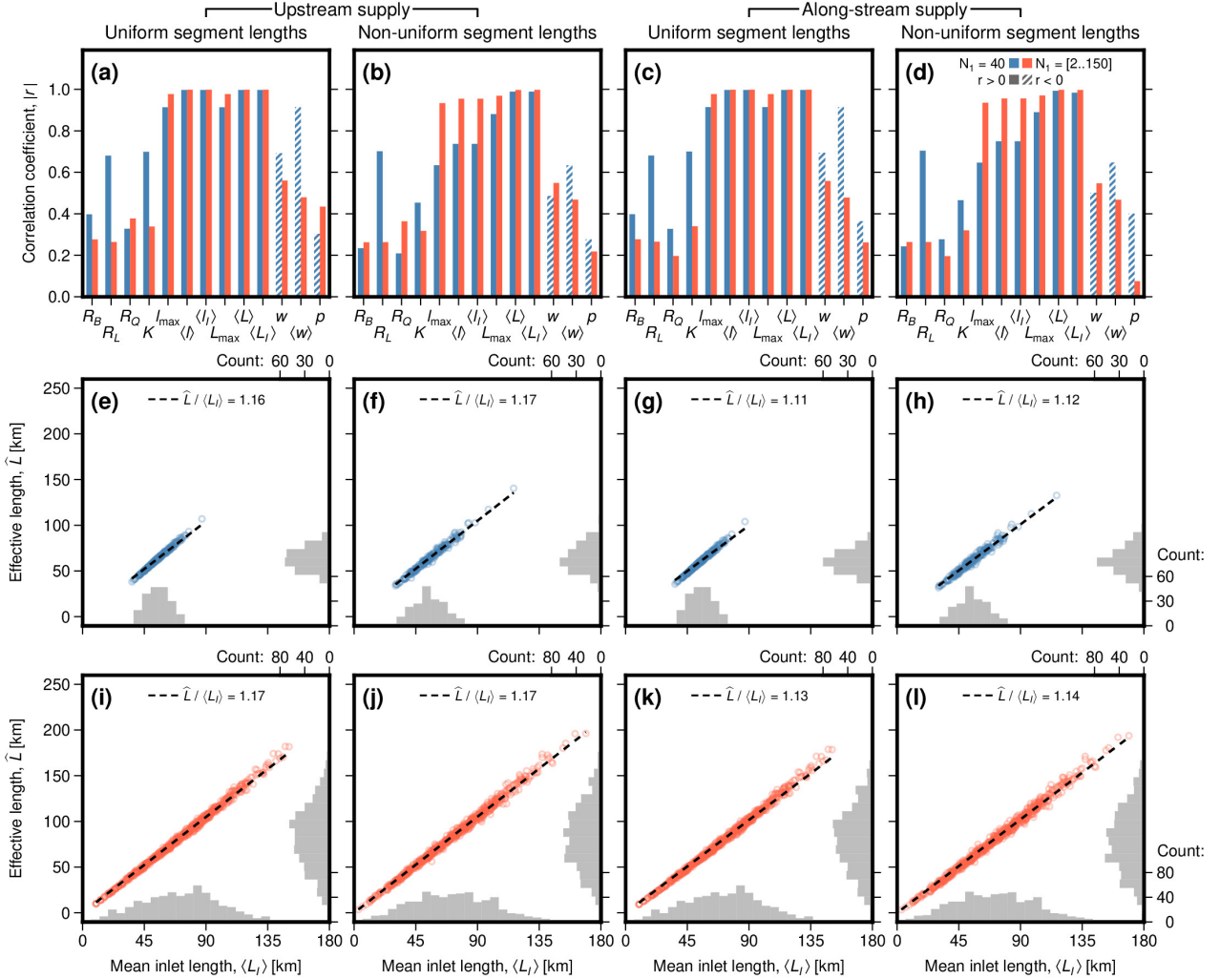


Figure S18. Counterpart to Figure 11, where valley width, B , increases downstream at the same rate as water discharge, Q_w , rather than being spatially uniform. Controls on the network effective length, \hat{L} , are shown for four network scenarios with: (a,e,i) uniform segment lengths with no along-stream supply of sediment and water; (b,f,j) non-uniform segment lengths with no along-stream supply of sediment and water; (c,g,k) uniform segment lengths with along-stream supply of sediment and water; (d,h,l) non-uniform segment lengths with along-stream supply of sediment and water. (a–d) Magnitude of Spearman's rank correlation coefficient, $|r|$, between \hat{L} and selected network properties. Blue bars represent sets of 200 networks each with 40 valley inlet segments; orange bars represent sets of 600 networks with 2–150 valley inlet segments. Solid bars correspond to positive trends while hatched bars correspond to negative trends. (e–h) Circles show \hat{L} as a function of mean length, $\langle L_I \rangle$, for each network in the sets of simulations with 40 valley inlet segments. Histograms show distributions of each variable. Dashed lines show best-fit linear relationship, constrained to pass through the origin. (i–l) As (e–h) for the sets of simulations with 2–150 valley inlet segments.

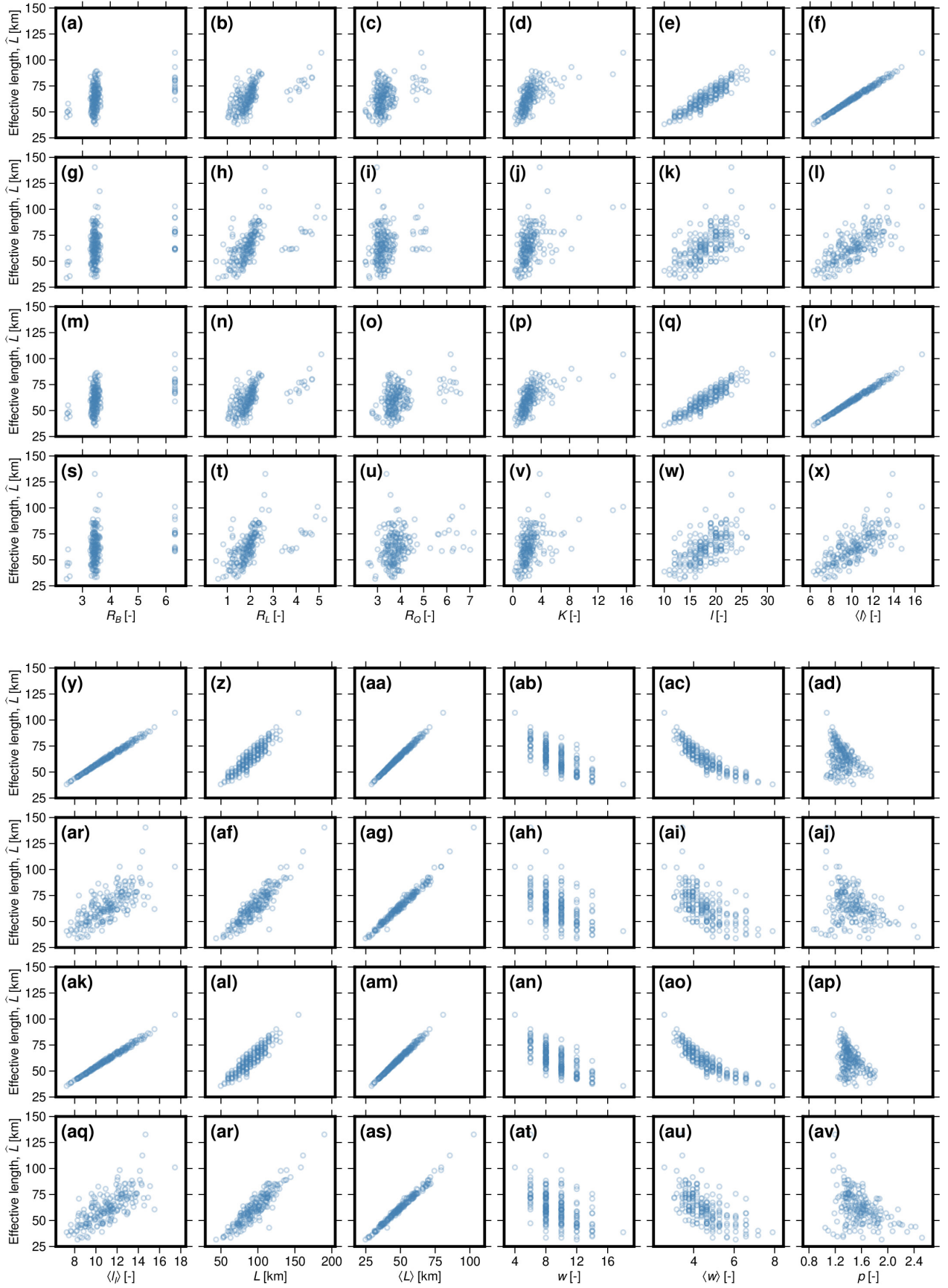


Figure S19. (Previous page.) Counterpart to Figure S5, where valley width, B , increases downstream at the same rate as water discharge, Q_w , rather than being spatially uniform. Network effective length, \hat{L} , is shown as function of various network properties for the set of networks with number of inlet segments, $N_1=40$. Four network scenarios are shown: (a–f) uniform segment lengths with no along-stream supply of sediment and water; (g–l) non-uniform segment lengths with no along stream supply of sediment and water; (m–r) uniform segment lengths with along stream supply of sediment and water; (s–x) non-uniform segment lengths with along-stream supply of sediment and water. (a, g, m, s) \hat{L} against bifurcation ratio, R_B . (b, h, n, t) \hat{L} against length ratio, R_L . (c, i, o, u) \hat{L} against discharge ratio, R_Q . (d, j, p, v) \hat{L} against Tokunaga’s K . (e, k, q, w) \hat{L} against maximum topological length, l . (f, l, r, x) \hat{L} against mean topological length, $\langle l \rangle$. (y, ae, ak, aq) \hat{L} against mean inlet topological length, $\langle l_I \rangle$. (z, af, al, ar) \hat{L} against maximum length, L . (aa, ag, am, as) \hat{L} against mean length, $\langle L \rangle$. (ab, ah, an, at) \hat{L} against maximum topological width, w . (ac, ai, ao, au) \hat{L} against mean topological width, $\langle w \rangle$. (ad, aj, ap, av) \hat{L} against downstream distance–discharge exponent, p .

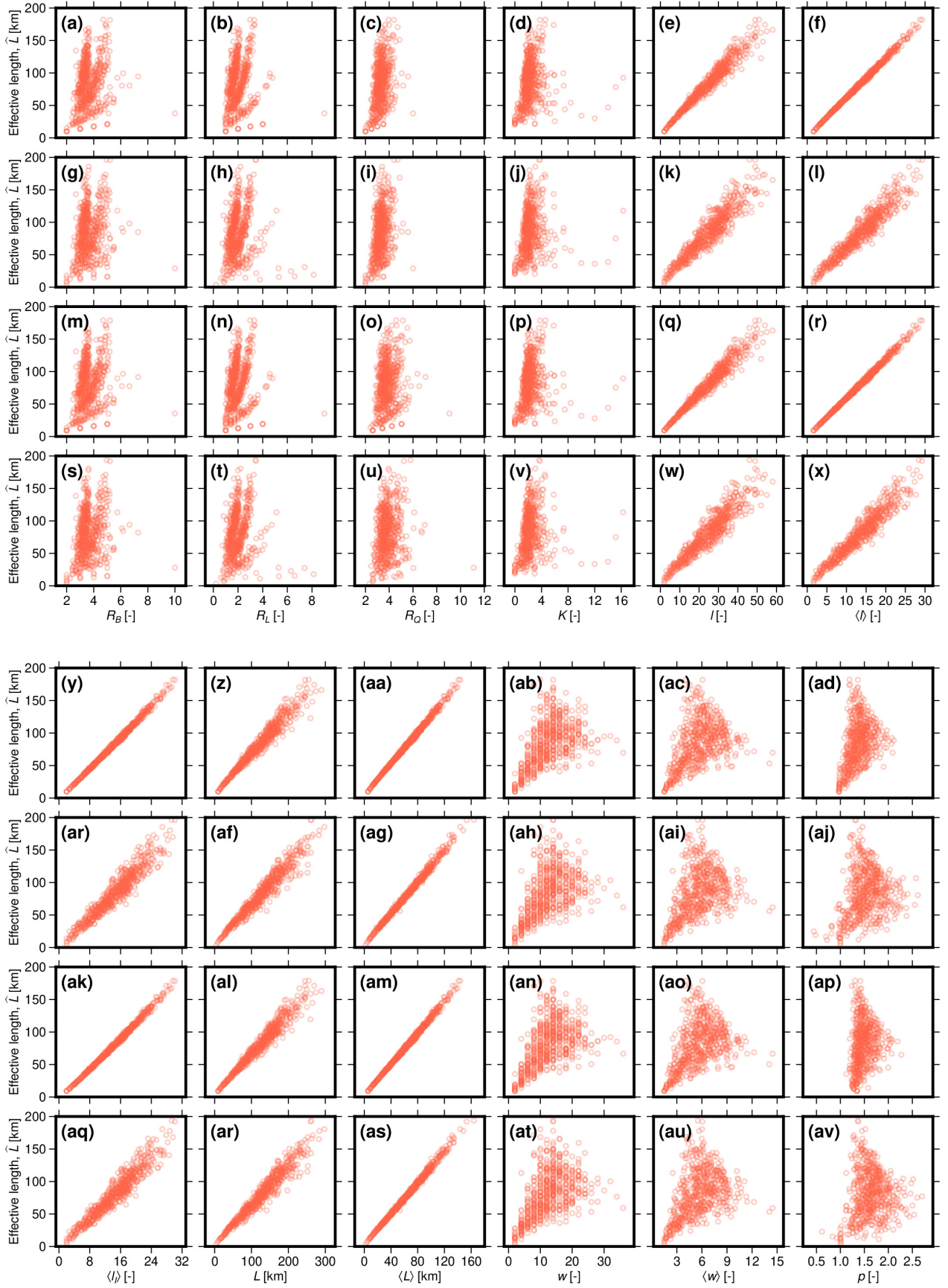


Figure S20. (Previous page.) Counterpart to Figure S6, where valley width, B , increases downstream at the same rate as water discharge, Q_w , rather than being spatially uniform. Network effective length, \hat{L} , is shown as function of various network properties for the set of networks with number of inlet segments, $N_1=2-150$. Four network scenarios are shown: (a–f) uniform segment lengths with no along-stream supply of sediment and water; (g–l) non-uniform segment lengths with no along stream supply of sediment and water; (m–r) uniform segment lengths with along stream supply of sediment and water; (s–x) non-uniform segment lengths with along stream supply of sediment and water. (a, g, m, s) \hat{L} against bifurcation ratio, R_B . (b, h, n, t) \hat{L} against length ratio, R_L . (c, i, o, u) \hat{L} against discharge ratio, R_Q . (d, j, p, v) \hat{L} against Tokunaga’s K . (e, k, q, w) \hat{L} against maximum topological length, l . (f, l, r, x) \hat{L} against mean topological length, $\langle l \rangle$. (y, ae, ak, aq) \hat{L} against mean inlet topological length, $\langle l_I \rangle$. (z, af, al, ar) \hat{L} against maximum length, L . (aa, ag, am, as) \hat{L} against mean length, $\langle L \rangle$. (ab, ah, an, at) \hat{L} against maximum topological width, w . (ac, ai, ao, au) \hat{L} against mean topological width, $\langle w \rangle$. (ad, aj, ap, av) \hat{L} against downstream distance–discharge exponent, p .

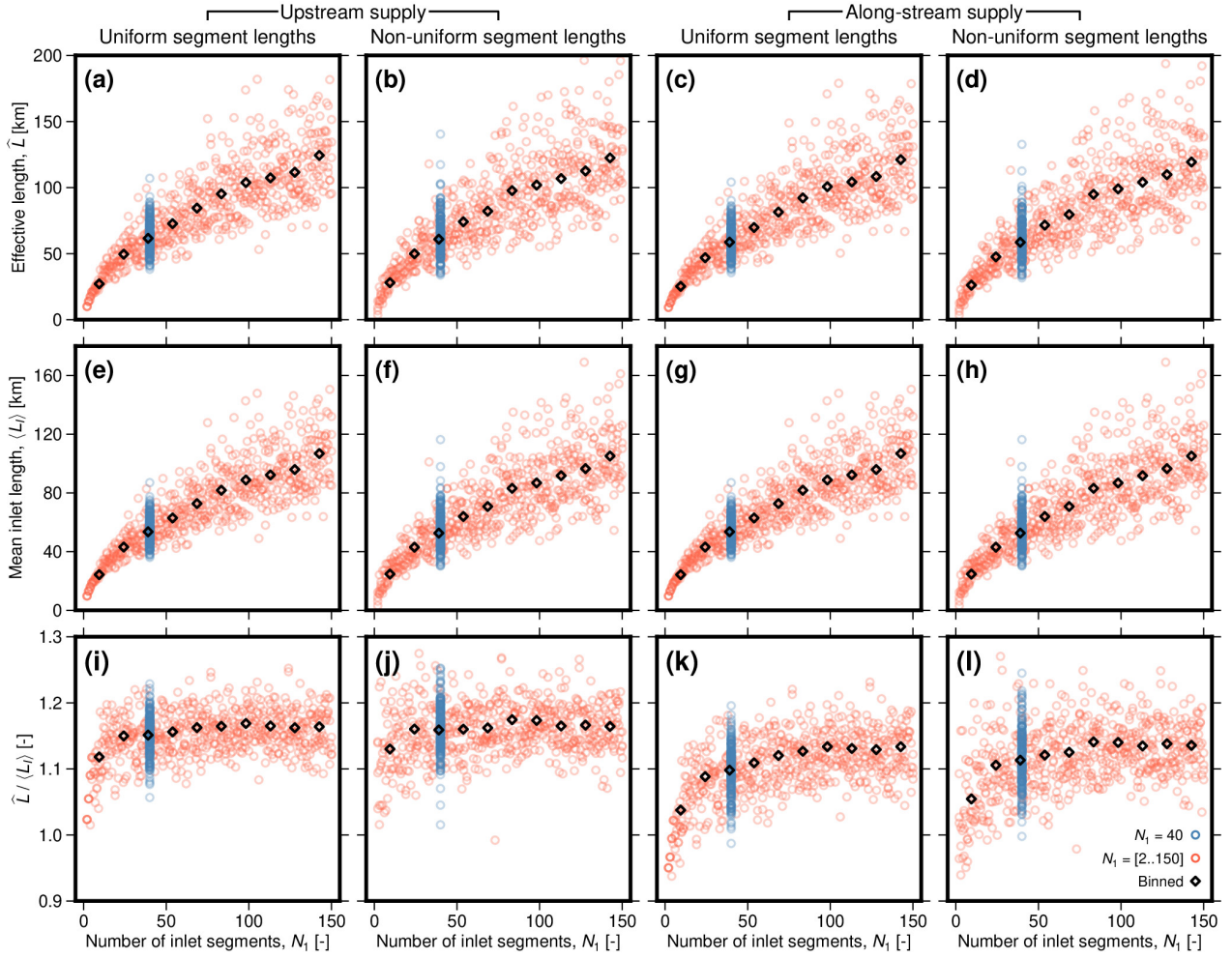


Figure S21. Counterpart to Figure 12, where valley width, B , increases downstream at the same rate as water discharge, Q_w , rather than being spatially uniform. (a–d) Network effective lengths, \hat{L} ; (e–h) mean inlet lengths, $\langle L_I \rangle$; and (i–l) their ratio as functions of the number of valley inlet segments, N_1 , for four network scenarios with: (a,e,i) uniform segment lengths with no along-stream supply of sediment and water; (b,f,j) non-uniform segment lengths with no along-stream supply of sediment and water; (c,g,k) uniform segment lengths with along-stream supply of sediment and water; (d,h,l) non-uniform segment lengths with along-stream supply of sediment and water. Circles represent individual networks; blue belong to set of simulations with N_1 fixed to 40, while orange belong to set with N_1 between 2 and 150. Diamonds represent binned values.

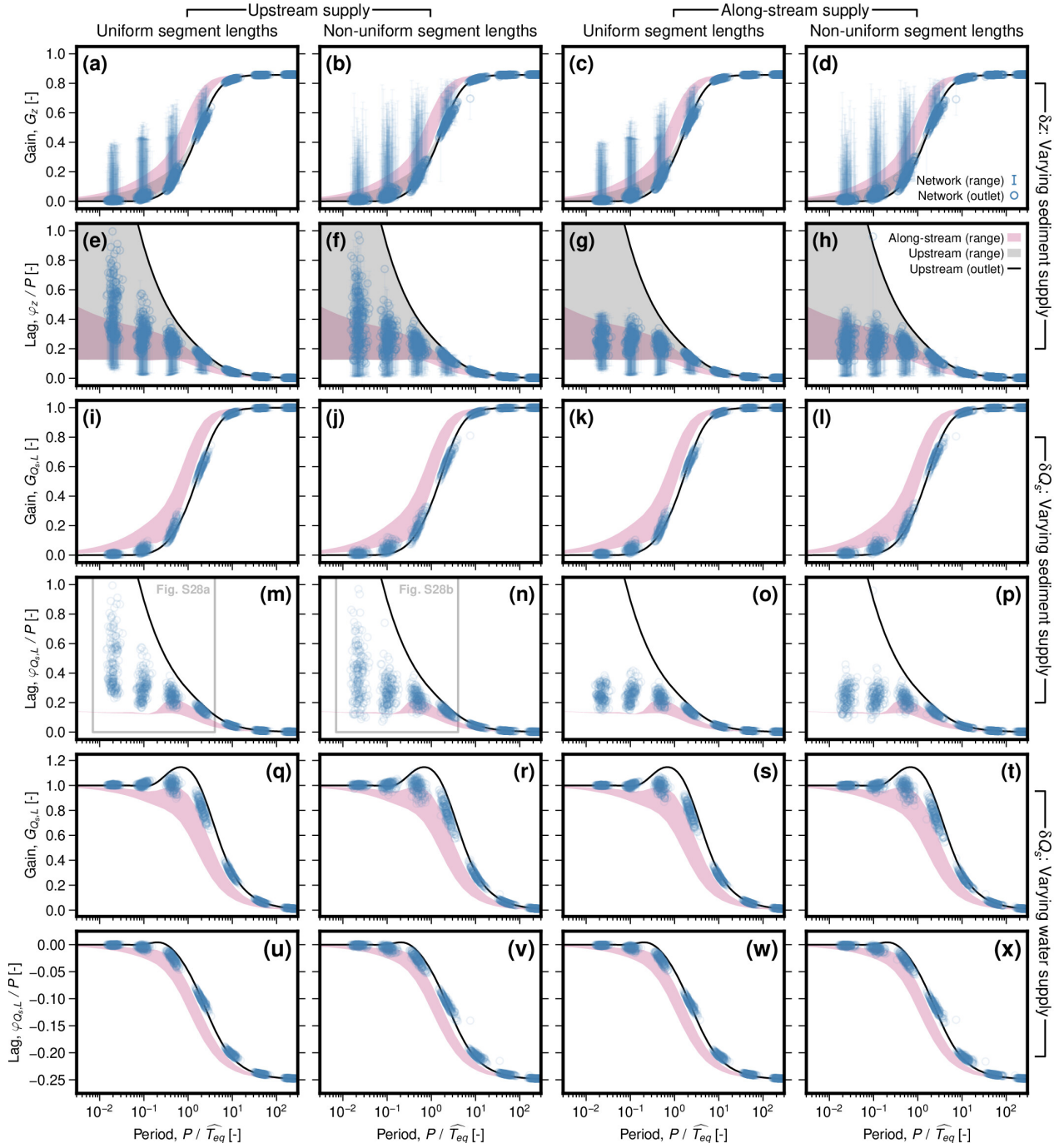


Figure S22. Counterpart to Figure 13, where valley width, B , increases downstream at the same rate as water discharge, Q_w , rather than being spatially uniform. Gain, G , and lag, φ , are shown as functions of forcing period, P , normalised to empirical equilibration time, \widehat{T}_{eq} , for the set of networks with number of inlet segments, $N_1=40$. Four network scenarios are shown: (a,e,i,m,q,u) uniform segment lengths with no along-stream supply of sediment and water; (b,f,j,n,r,v) non-uniform segment lengths with no along-stream supply of sediment and water; (c,g,k,o,s,w) uniform segment lengths with along-stream supply of sediment and water; (d,h,l,p,t,x) non-uniform segment lengths with along-stream supply of sediment and water. (a–d) Elevation gain, G_z , in response to variation in sediment supply. Circles represent value at the network outlet, where error bars represent range throughout network. Black line and grey band represent value at outlet and range along stream, respectively, for single-segment case with all water and sediment supplied at the inlet (according to analytical solution of M^cNab et al., 2023). Pink band represents range along stream for single-segment case with along-stream supply of water and sediment, for power-law exponents $p_{x,Q_w} = p_{x,Q_s} = 0.8\text{--}2.4$. (e–h) As (a–d) for elevation lag. (i–p) As (a–h) for sediment-discharge gain, G_{Q_s} , and lag, φ_{Q_s} . Note that only values for the outlet are shown. Panels (i–l) are the same as Figure S16e–h. (q–x) As (i–p) for response to variation in water supply. Equivalent results for the set of networks with $N_1=2\text{--}150$ are shown in Figure S23. Equivalent results to panels (a–h) for variation in water supply are shown in Figure S24, and for the set of networks with $N_1=2\text{--}150$ are shown in Figure S25.

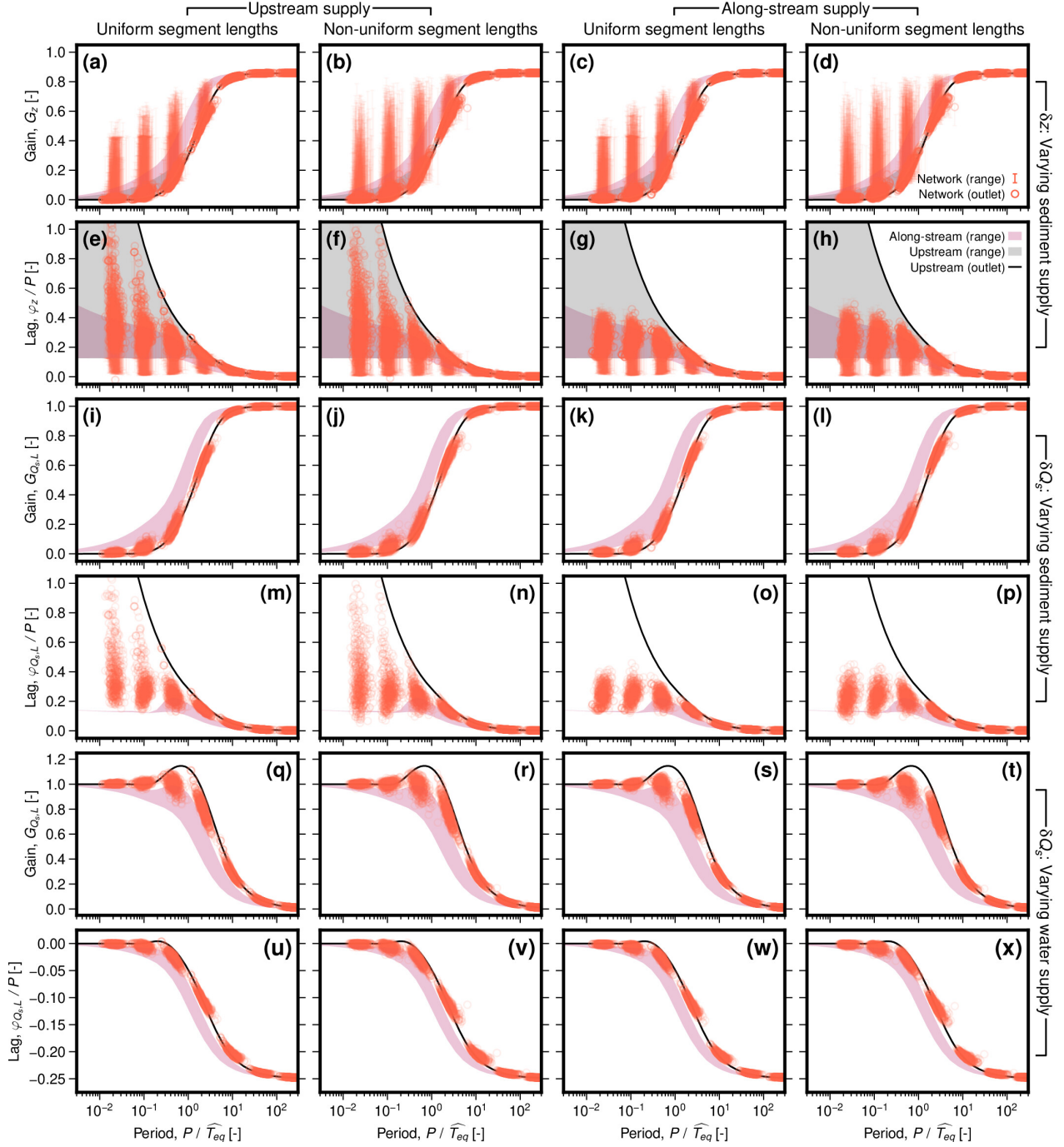


Figure S23. Counterpart to Figure S7, where valley width, B , increases downstream at the same rate as water discharge, Q_w , rather than being spatially uniform. Gain, G , and lag, φ , are shown as functions of forcing period, P , normalised to empirical equilibration time, \widehat{T}_{eq} , for the set of networks with number of inlet segments, $N_1=2-150$. Four network scenarios are shown: (a,e,i,m,q,u) uniform segment lengths with no along-stream supply of sediment and water; (b,f,j,n,r,v) non-uniform segment lengths with no along-stream supply of sediment and water; (c,g,k,o,s,w) uniform segment lengths with along-stream supply of sediment and water; (d,h,l,p,t,x) non-uniform segment lengths with along-stream supply of sediment and water. (a–d) Elevation gain, G_z , in response to variation in sediment supply. Circles represent value at the network outlet, where error bars represent range throughout network. Black line and grey band represent value at outlet and range along stream, respectively, for simple case with all water and sediment supplied at the inlet (according to analytical solution of M^cNab et al., 2023). Pink band represents range along stream for simple case with along-stream supply of water and sediment, for power-law exponents $p_{x,Q_w} = p_{x,Q_s} = 0.8-2.4$. (e–h) As (a–d) for elevation lag. (i–p) As (a–h) for sediment-discharge gain, G_{Q_s} , and lag, φ_{Q_s} . Note that only values for the outlet are shown. Panels (i–l) are the same as Figure S17e–h. (q–x) As (i–p) for response to variation in water supply. Equivalent results to panels (a–h) for variation in water supply are shown in Figure S25.

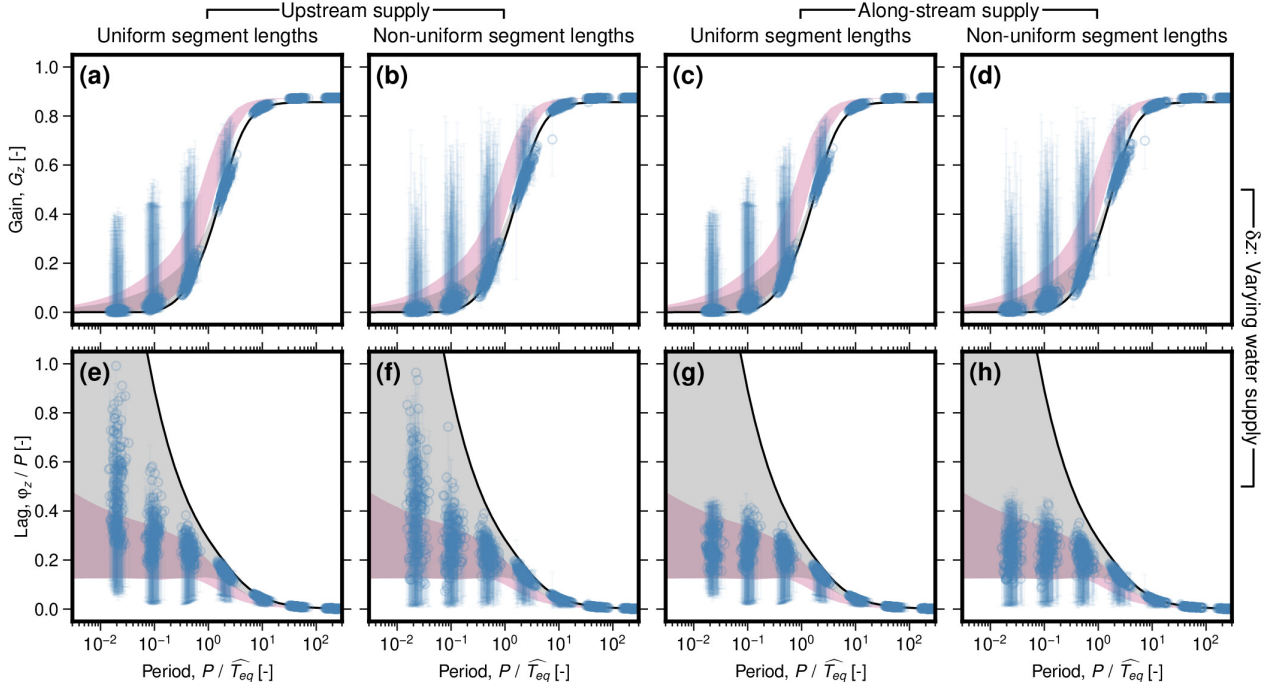


Figure S24. Counterpart to Figure S8, where valley width, B , increases downstream at the same rate as water discharge, Q_w , rather than being spatially uniform. Gain, G , and lag, φ , are shown as functions of forcing period, P , normalised to empirical equilibration time, \widehat{T}_{eq} , for the set of networks with number of inlet segments, $N_1=40$. Four network scenarios are shown: (a,e) uniform segment lengths with no along-stream supply of sediment and water; (b,f) non-uniform segment lengths with no along-stream supply of sediment and water; (c,g) uniform segment lengths with along-stream supply of sediment and water; (d,h) non-uniform segment lengths with along-stream supply of sediment and water. (a–d) Elevation gain, G_z , in response to variation in water supply. Circles represent value at the network outlet, where error bars represent range throughout network. Black line and grey band represent value at outlet and range along stream, respectively, for simple case with all water and sediment supplied at the inlet (according to analytical solution of M^cNab et al., 2023). Pink band represents range along stream for simple case with along-stream supply of water and sediment, for power-law exponents $p_{x,Q_w} = p_{x,Q_s} = 0.8\text{--}2.4$. (e–h) As (a–d) for elevation lag.

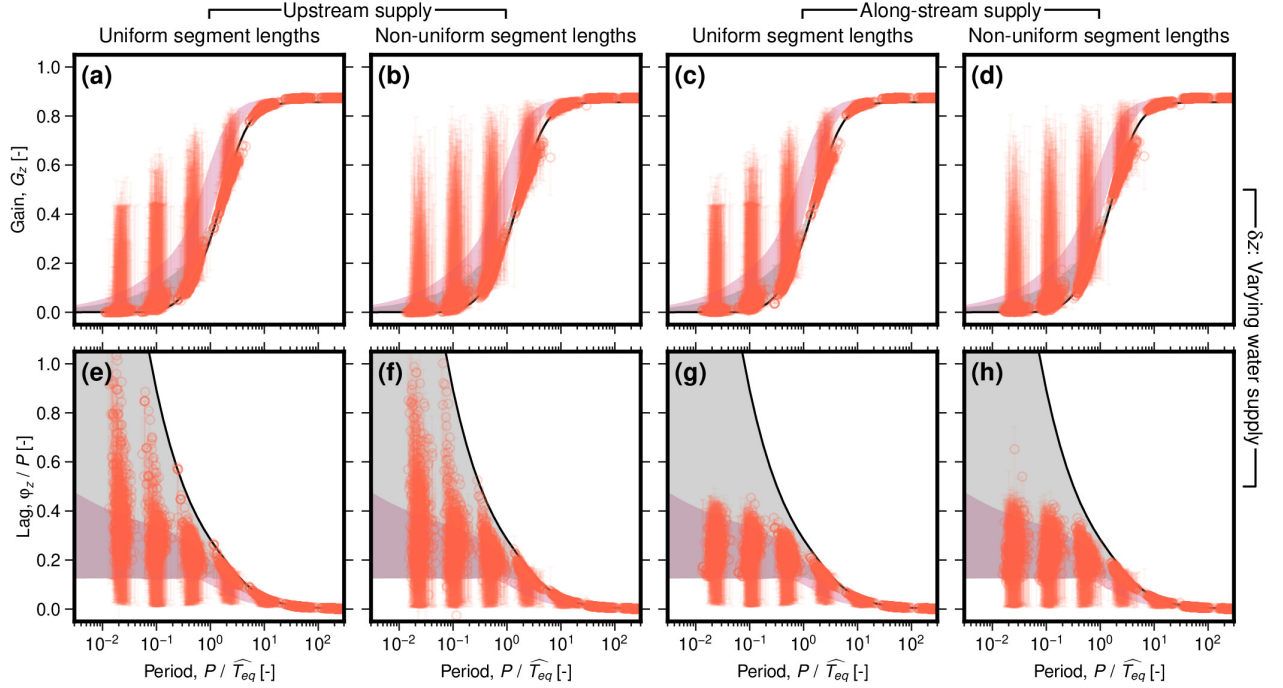


Figure S25. Counterpart to Figure S9, where valley width, B , increases downstream at the same rate as water discharge, Q_w , rather than being spatially uniform. Gain, G , and lag, φ , are shown as functions of forcing period, P , normalised to empirical equilibration time, \widehat{T}_{eq} , for the set of networks with number of inlet segments, $N_1=2-150$. Four network scenarios are shown: (a,e) uniform segment lengths with no along-stream supply of sediment and water; (b,f) non-uniform segment lengths with no along-stream supply of sediment and water; (c,g) uniform segment lengths with along-stream supply of sediment and water; (d,h) non-uniform segment lengths with along-stream supply of sediment and water. (a–d) Elevation gain, G_z , in response to variation in water supply. Circles represent value at the network outlet, where error bars represent range throughout network. Black line and grey band represent value at outlet and range along stream, respectively, for simple case with all water and sediment supplied at the inlet (according to analytical solution of M^cNab et al., 2023). Pink band represents range along stream for simple case with along-stream supply of water and sediment, for power-law exponents $p_{x,Q_w} = p_{x,Q_s} = 0.8-2.4$. (e–h) As (a–d) for elevation lag.

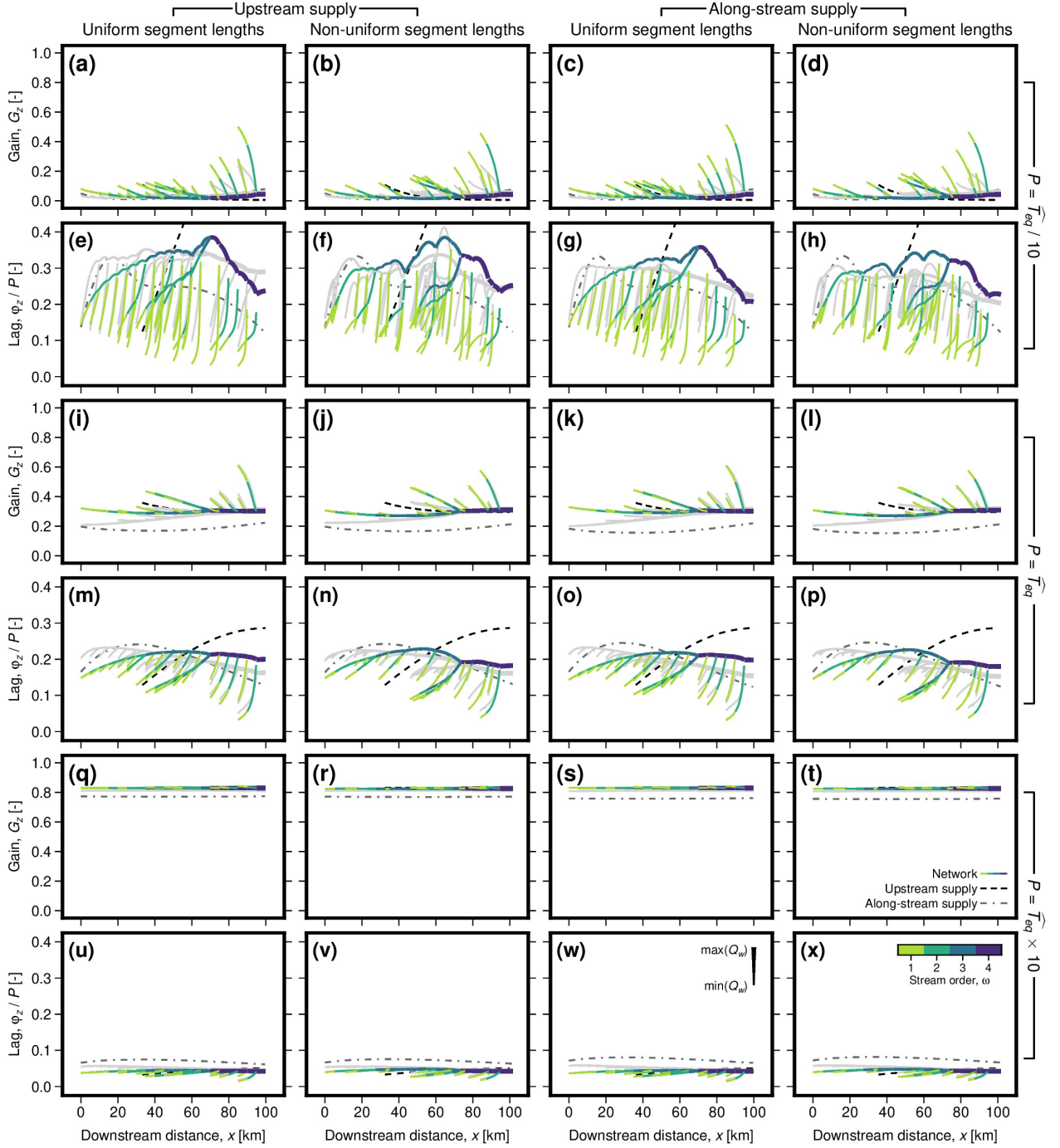


Figure S26. Counterpart to Figure 15, where valley width, B , increases downstream at the same rate as water discharge, Q_w , rather than being spatially uniform. Gain, G_z , and lag, ϕ_z/P , as functions of downstream distance for three forcing periods and networks with: (a,e,i,m,q,u) uniform and (b,f,j,n,r,v) non-uniform segment lengths and upstream supply of sediment and water; (c,g,k,o,s,w) uniform and (d,h,l,p,t,x) non-uniform segment lengths with along-stream supply of sediment and water. (a–d) G_z as function of downstream distance where $P = \widehat{T}_{eq}/10$. Solid, coloured lines show network segments shaded by stream order, with line thickness scaled by water discharge (see key in panel (w)). For comparison, solid grey lines show equivalent case with uniform valley width. Black dashed line shows single-segment case where all sediment and water is supplied at the valley inlet, with length equal to the network empirical effective length, \widehat{L} (according to analytical solution of M^cNab et al., 2023). Grey dashed/dotted line shows single-segment, along-stream supply case, with power-law exponent equal to the network’s best-fitting exponent, and with length equal to the network’s maximum length. (e–h) As (a–d) for ϕ_z . (i–p) As (a–h) for $P = \widehat{T}_{eq}$. (q–x) As (a–h) for $P = \widehat{T}_{eq} \times 10$.

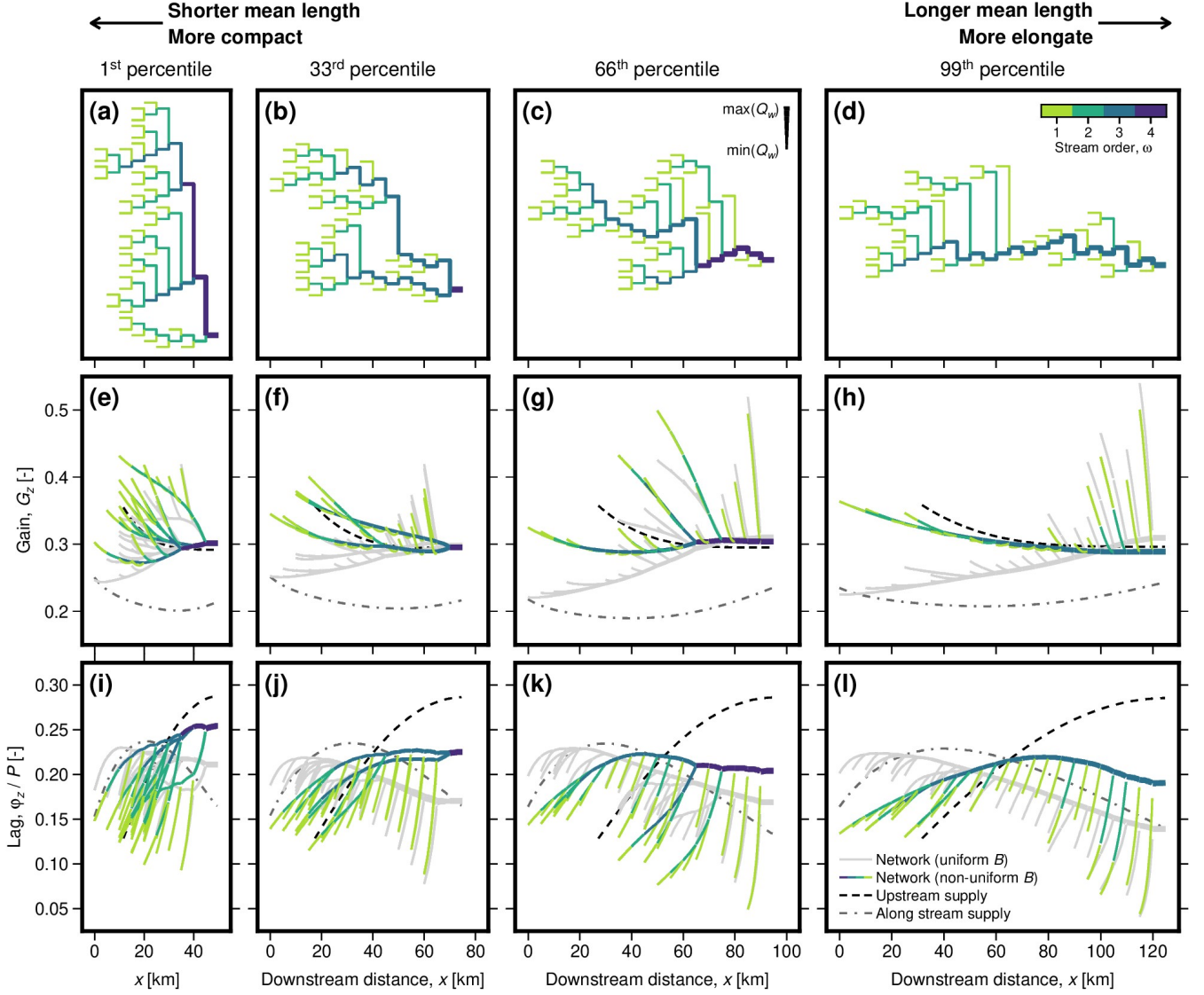


Figure S27. Counterpart to Figure 16, where valley width, B , increases downstream at the same rate as water discharge, Q_w , rather than being spatially uniform. Gain, G_z , and lag, φ_z/P , are shown as functions of downstream distance for networks with a range of mean lengths. From the set of networks with number of inlet segments, $N_1=40$, we select networks with mean lengths corresponding to the 1st (i.e. shortest) percentile (a,e,i), 33rd percentile (b,f,j), 66th percentile (c,g,k), and 99th (i.e. longest) percentile. (a–d) Schematic network planforms, where colour indicates stream order. Vertical axis has no physical meaning; planforms are intended only to illustrate relationships between segments. (e–h) G_z as function of downstream distance. Solid, coloured lines show network segments shaded by stream order, with line thickness scaled by water discharge (see key in panel (c)). For comparison, solid grey lines show equivalent case with uniform valley width. Black dashed line shows single-segment, upstream supply case, with length equal to the network empirical effective length, \hat{L} (according to analytical solution of M^cNab et al., 2023). Grey dashed/dotted line shows single-segment, along-stream supply case where sediment and water follow power law with exponent equal to the network’s best-fitting exponent, and with length equal to the network’s maximum length. (i–l) As (a–d) for φ_z .

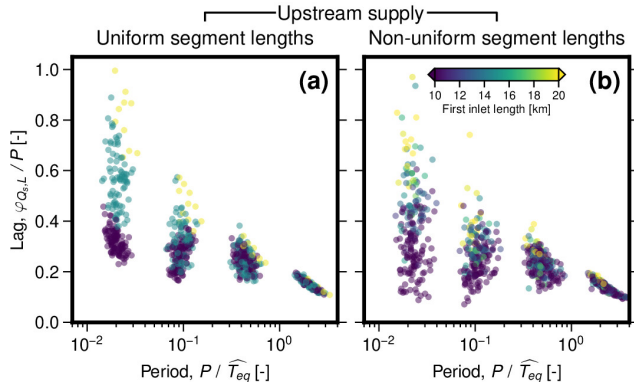


Figure S28. Counterpart to Figure 17, where valley width, B , increases downstream at the same rate as water discharge, Q_w , rather than being spatially uniform. Sediment-discharge lag at the network outlet, $\varphi_{Q_{s,L}}$, is shown as a function of forcing period, P , normalised by empirical equilibration time, \widehat{T}_{eq} , with focus on shorter forcing periods (see boxes on Figure S22 for position within wider parameter space). Lag measurements for each network are shaded by distance upstream to the first inlet segment. (a) Networks with only upstream supply and uniform segment lengths. Uniform segment lengths result in three populations in which the first inlet segment occurs two, three or four segments upstream from the outlet. (b) Networks with only upstream supply and non-uniform segment lengths.

References

- McNab, F., Schildgen, T. S., Turowski, J. M., and Wickert, A. D.:
Diverse responses of alluvial rivers to periodic environmental
change, *Geophysical Research Letters*, 50, e2023GL103 075,
5 <https://doi.org/10.1029/2023GL103075>, 2023.